Effect of Retained Austenite on the Corrosion Behaviour of Q&P Processed Martensitic Stainless Steels

Master Thesis

Adnan Akman

Effect of Retained Austenite on the Corrosion Behaviour of Q&P Processed Martensitic Stainless Steels

Master Thesis

Thesis

submitted to the

Delft University of Technology

in partial fulfillment of the requirements for the degree of

Master of Science in Materials Science and Engineering

by

Adnan Akman

December 2021, Delft

Keywords: corrosion, Q&P treatment, stainless steel, microstructure

Supervisor: Dr. Yaiza Gonzalez-Garcia

Committee members:

Dr. Yaiza Gonzalez-Garcia

Prof. Dr. Jilt Sietsma

Dr. Aytac Yilmaz

Master Thesis: *Effect of Retained Austenite on the Corrosion Behaviour of Q&P Processed Martensitic Stainless Steels*

I am not leaving a spiritual legacy of dogmas, unchangeable petrified directives. My spiritual legacy is science and reason.

Mustafa Kemal Atatürk

Acknowledgements

Firstly, I would like to express my heartfelt gratitude to Dr. Yaiza Gonzalez-Garcia for her guidance and constant support during the trying times of COVID-19.

I would also like to extend my thanks to Dr. Aytac Yilmaz, for his patient guidance. I would also like to thank Gaojie Li, for her assistance with sample preparation and many thanks to Agnieszka Kooijman for her support in the electrochemical experiments.

I am very thankful to all my friends at the Materials Science and Engineering department, especially the ones in Corrosion Technology and Electrochemistry group.

Finally, I would like to thank my parents for their constant support throughout my studies.

Abstract

The fuel consumption of cars has become an important issue in the development of new materials. These developments resulted in the generation of new grades of steel for the automotive industry. In particular, new advanced high strength steels (AHSS) have been developed for the automotive industry to lower fuel consumption (with weight reduction) by combining strength with formability. Especially, quenching and partitioning (Q&P) steels from 3rd generation AHSS can exhibit significant strength and ductility balance by combining martensite with retained austenite. Recently, there has been a new interest in applying the Q&P treatment to stainless steels, in particular martensitic stainless steel. For the automotive industry, the development in Q&P treated martensitic stainless steel can be a game-changer. The mechanical properties of Q&P treated commercial martensitic stainless steels have been widely researched. Unlike mechanical behaviour, the corrosion behaviour of Q&P treated martensitic stainless steel has not been investigated deeply. The effect of environmental factors or the effect of microstructure on the corrosion performance of Q&P processed martensitic stainless steel needs to be studied.

This master thesis aims to identify the effect of microstructural constituents (retained austenite, primary and fresh martensite) on the corrosion response of Q&P treated martensitic stainless steels. To this end, an experimental approach is taken for this project. This work aims to create a relationship between heat treatment, microstructure, and the resulting corrosion properties. As an experimental path, open circuit potential (OCP), electrochemical impedance spectroscopy (EIS), potentiodynamic polarization and Mott-Schottky experiments were carried out in 3.5 wt.% NaCl solution to reveal the corrosion response and passive film properties of the Q&P microstructures. In addition, X-ray photoelectron spectroscopy (XPS) was performed to analyze the chemical composition and fractions of oxide layers in the passive layer. Results demonstrate a phase dependency for the corrosion performance of Q&P treated martensitic stainless steels.

Nomenclature

$AHSS$	Advanced high strength steel
DP	Dual phase
CP	Complex phase
$TRIP$	Transformation induced plasticity
$TWIP$	Twinning induced plasticity
$Q\&P$	Quenching and partitioning
$Q\&T$	Quenching and tempering
G	Gibbs free energy $[J/mol]$
H	Enthalpy $[J/mol]$
S	Entropy $[J/molK]$
n	number of elementary charges
E	Electromotive force $[J/mol]$
R	Gas constant = 8.3145 $[J/molK]$
C_{Red}	Reduced bulk molecule concentration $[mol]$
C_{Ox}	Oxidized bulk molecule concentration $[mol]$
v	Reaction rate $[mol/m^2s]$
j	Current density $[A/m^2]$
E_{eq}	Equilibrium potential $[V]$
j_0	Exchange current density $[A/m^2]$
η	Overpotential $[V]$
α_a	Anodic charge transfer coefficient
α_c	Cathodic charge transfer coefficient
a	Molar Mass $[kg/mol]$
ρ	Density $[kg/m^3]$

EPR	Electrochemical potentiodynamic reactivation
OCP	Open circuit potential
EIS	Electrochemical impedance spectroscopy
XPS	X-ray photoelectron spectroscopy
AC	Alternating current

Contents

Acknowledgements vii

Abstract ix

Nomenclature xi

List of Figures xv

List of Tables xvii

1 Introduction 1
1.1 Advanced High Strength Steels 1

2 Background 3
2.1 The Quenching and Partitioning (Q&P) Process 3
2.2 Q&P Process of Stainless Steels 6
2.3 Corrosion 10
2.4 Corrosion Electrochemistry 10
2.5 Thermodynamics 11
2.6 Kinetics 12
2.7 Pitting Corrosion 13
2.8 Corrosion Behaviour of Q&P Stainless Steels 15
2.9 Passivation and Oxide Film Properties 17
2.10 Research Approach and Thesis Focus 18

3 Experimental Procedure 19
3.1 Microstructure Characterization 19
3.1.1 Material 19
3.1.2 Design of the Q&P Treatment 20
3.1.3 Dilatometry 23
3.1.4 Sample Preparation 24
3.1.5 Investigation of the Microstructure 24
3.2 Electrochemical Analysis 25
3.2.1 Sample Preparation 25
3.2.2 Electrochemical Setup 25
3.2.3 Electrochemical Experiments 26
3.3 Passive Layer Analysis 27

4 Results and Discussion 29
4.1 Application of the Q&P Treatment 29
4.2 Electrochemical Measurements 30
4.3 Passive Layer Analysis 39

4.4 Phase Dependency of Corrosion and Passivity 43

5 Conclusions and Recommendations **47**
5.1 Conclusions 47
5.2 Recommendations 49
References 50

List of Figures

1.1 Summary of tensile strength and elongation data for different classes of conventional and advanced high strength steel grades. 1

2.1 Schematic heat-treatment diagram of the quenching and partitioning (Q&P) process. 4
2.2 Gibbs free-energy vs. composition diagram that satisfies the CCE requirement. 5
2.3 Nominal stress-strain curve of AISI 410 steels after Q&P and Q&T treatment 7
2.4 Room temperature stress-strain curves for Q&P treated stainless steels partitioned at 723 K (450 °C). (b) Summarized tensile properties of Q&P specimens partitioned at 723 K (450 °C) and 573 K (300 °C). . . 7
2.5 TEM images and diffraction pattern for the 450 °C - 10 minutes partitioned martensitic stainless steel. 8
2.6 Pourbaix diagram for $Fe - H_2O$ system at 25 °C. 12
2.7 Schematic representing the microstructure of Q&T and Q&P structures. 16

3.1 Phase mass fraction (BPW(*)) vs. temperature graph for the studied alloy. 20
3.2 Overview of the Q&P heat treatment used in this study. 23
3.3 An example of the completed sample for electrochemical experiments. 25
3.4 Electrochemical cell setup. 26

4.1 Potentiastatic polarization curve at applied potential of -300 mV (vs. OCP) for 10 minutes in 3.5 wt.% NaCl solution. 30
4.2 The open circuit potentials of commercial martensitic stainless steel (AISI 420) and Q&P treated martensitic stainless steels in 3.5 wt.% NaCl solution. 31
4.3 Potentiodynamic polarization plots of commercial martensitic stainless steel (AISI 420) and Q&P treated martensitic stainless steels in 3.5 wt.% NaCl solution. 32
4.4 Pitting potentials (E_{pit}) of the stainless steel samples based on potentiodynamic polarization curves. 33
4.5 Passivation current density (i_{pass}) of the stainless steel samples based on potentiodynamic polarization curves. 34
4.6 Nyquist plots of commercial martensitic stainless steel (AISI 420) and Q&P treated martensitic stainless steels in 3.5 wt.% NaCl solution. . 34

4.7 Bode impedance plots of commercial martensitic stainless steel (AISI 420) and Q&P treated martensitic stainless steels in 3.5 wt.% NaCl solution. 35
4.8 Phase angle plot of commercial martensitic stainless steel (AISI 420) and Q&P treated martensitic stainless steels in 3.5 wt.% NaCl solution. 35
4.9 Equivalent circuit proposed for modelling the electrochemical response of commercial martensitic stainless steel (AISI 420) and Q&P treated martensitic stainless steels. 36
4.10 Mott-Schottky plots for the passive film formed on Q&P treated martensitic stainless steels in 3.5 wt.% NaCl solution. 37
4.11 Space charge region (SCR) and Helmholtz (HL) double layer at the semiconductor-electrolyte interface. 38
4.12 Experimental Fe 2p spectrum from the XPS measurement and corresponding fitting of the spectrum for the QT113. 41
4.13 Experimental Fe 2p spectrum from the XPS measurement and corresponding fitting of the spectrum for the QT183. 41
4.14 Experimental Cr 2p spectrum from the XPS measurement and corresponding fitting of the spectrum for the QT113. 42
4.15 Experimental Cr 2p spectrum from the XPS measurement and corresponding fitting of the spectrum for the QT183. 42

List of Tables

3.1 Chemical composition (wt.%) of Q&P treated steel sample. 19
3.2 Selected quenching temperatures and untransformed austenite fractions. 22

4.1 Phase fractions of Q&P processed specimens with different quenching temperatures. 29
4.2 Corrosion current density (i_{corr}), corrosion potential (E_{corr}) and pitting potential (E_{pit}) values of Q&P processed and AISI 420 steels calculated from the potentiodynamic polarization experiments. 31
4.3 The fitting values of the equivalent circuit components for AISI 420 and Q&P processed martensitic stainless steels. 36
4.4 Donor density and flat band potential values obtained from Mott-Schottky analysis. 38
4.5 Fractions of the passive layer calculated from the fitting of Fe 2p spectrum. 40
4.6 Fractions of the passive layer calculated from the fitting of Cr 2p spectrum. 40

1

Introduction

1.1. Advanced High Strength Steels

The fuel consumption of cars has become an important issue in the development of new materials and these developments resulted in the generation of new steel grades. The developments started with the micro-alloyed steels and new grades appeared for the automotive industry. Recently, advanced high strength steel (AHSS) has been developed for automotive components (A-pillars, B-pillars, side-impact beams, bumpers) to lower fuel consumption (with a weight reduction) by combining strength with ductility. In particular, quenching and partitioning (Q&P) steels from 3rd generation AHSS can exhibit significant strength and ductility balance compared to dual-phase (DP), complex phase (CP), transformation induced plasticity (TRIP) steels from 1st generation AHSS. In addition, Q&P steels are not costly as Twinning Induced Plasticity (TWIP) steels from 2nd generation AHSS. It is apparent that, Q&P processed steels from 3rd generation AHSS is filling the gap between 1st and 2nd generation AHSS as shown in Figure 1.1 [1].

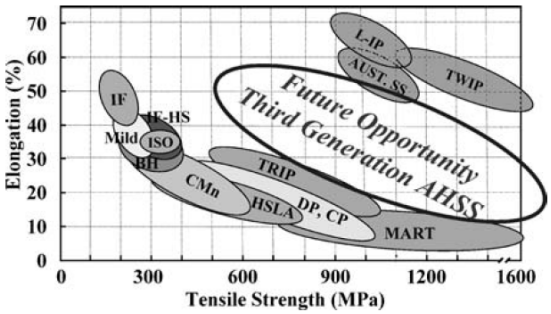

Figure 1.1: Summary of tensile strength and elongation data for different classes of conventional and advanced high strength steel grades [1].

1

The Q&P process proposed by Speer et al. [2] in 2003, and the relationship between microstructure and properties of Q&P steels have been investigated by many researchers. Recently, there has been a new interest in applying the Q&P treatment to stainless steels, in particular, martensitic stainless steel [3].

For the automotive industry, the development in Q&P treated martensitic stainless steels can be a game-changer. The mechanical properties of Q&P treated commercial martensitic stainless steels (AISI 410 and AISI 420) [4, 5] have been widely researched by many researchers to combine strength with ductility. According to the literature, the mechanical properties of the martensitic stainless steels can be improved with the Q&P process by combining the strength of the martensite with the ductility of the retained austenite. Unlike mechanical behaviour, the corrosion behaviour of Q&P treated martensitic stainless steel has not been investigated deeply. The effect of environmental factors or the effect of microstructure on the corrosion performance of Q&P martensitic stainless steel needs to be studied.

The thesis aims to create a relation between microstructure and the corrosion behaviour of Q&P treated martensitic stainless steels. As an experimental path, open circuit potential (OCP), potentiodynamic polarization, electrochemical impedance spectroscopy (EIS) were performed in 3.5 wt.% NaCl to understand the corrosion response of Q&P treated martensitic stainless steels and Mott-Schottky analysis were performed in 3.5 wt.% NaCl to reveal the passive film properties. In addition, X-ray photoelectron spectroscopy (XPS) was conducted to analyze the chemical composition of different types of oxides in the passive layer of Q&P treated martensitic stainless steels.

2

Background

2.1. The Quenching and Partitioning (Q&P) Process

Usually, heat treatment methods include a variety of techniques to improve the properties of steel. For centuries, quenching and tempering (Q&T) treatment has been applied to improve the mechanical properties of steels. Q&T process involves austenitising, quenching and tempering stages. The Q&T process starts with austenitising to allow the phase transformation of the initial microstructure into austenite. In this stage, the carbon in the austenite can dissolve completely at high temperatures. The austenitising stage is followed by quenching and this step is essential to form desired microstructural features in steel. If the austenitized steel is cooled rapidly, the carbon in austenite does not have enough time to diffuse out. This rapid cooling process is called quenching. In quenching, the trapped carbon atoms distort the lattice structure, due to this distortion a new type of microstructure is formed and called martensite. However, the distorted martensite creates a barrier for the dislocation movement and the limitation in the dislocation movement reduces the ductility of the steel. In order to improve ductility, the quenched steel needs to be treated and this is done by tempering. The tempering process reduces the hardness and strength slightly but increases ductility and toughness significantly. The quenched steels consist of martensite and a small amount of retained austenite (when steel is not quenched to the martensite finish temperature) in their microstructure. The small amount of retained austenite in Q&T steels vanish with tempering treatment [6, 7]. However, high mechanical properties and ductility combination could be obtained at the same time with a mixture of martensite and retained austenite in steels by applying a special heat treatment technique called Quenching and Partitioning (Q&P) [2].

2

In 2003, Speer et al. [2] suggested a heat treatment process called Quenching and Partitioning (Q&P). Q&P is a multi-step heat treatment route that produces austenite and martensite mixture to meet the desired combinations of strength and formability. The Q&P process includes cooling and heating steps, and an overview of the typical Q&P process is displayed in Figure 2.1 [8]. Firstly, the Q&P process starts with austenitising or intercritical annealing to set an initial austenite fraction, followed by interrupted quenching to a specific temperature between the martensite start temperature (M_s) and martensite finish temperature (M_f) to produce the desired martensite and untransformed austenite fractions. Then, austenite stabilization before final cooling to room temperature is obtained via carbon partitioning from carbon supersaturated martensite to austenite. The partitioning treatment can be performed at the same temperature as the quench temperature (one-step Q&P), or it can be performed at a higher temperature than the quench temperature (two-step Q&P) [9]. The carbon enrichment of the untransformed austenite during partitioning lowers its M_s temperature and this enrichment stabilizes the austenite upon cooling to room temperature. If the austenite is not sufficiently enriched with carbon, some part of it can transform into fresh martensite during the final cooling to room temperature. The final microstructure after the Q&P process typically consists of:

- Primary martensite: Primary martensite is formed during the initial quench to room temperature and tempered during the partitioning stage.
- Retained austenite: Retained austenite stabilized to room temperature by carbon diffusion during the partitioning stage.
- Fresh martensite: Fresh martensite can only form via final quench to room temperature when the untransformed austenite is not enriched sufficiently with carbon.

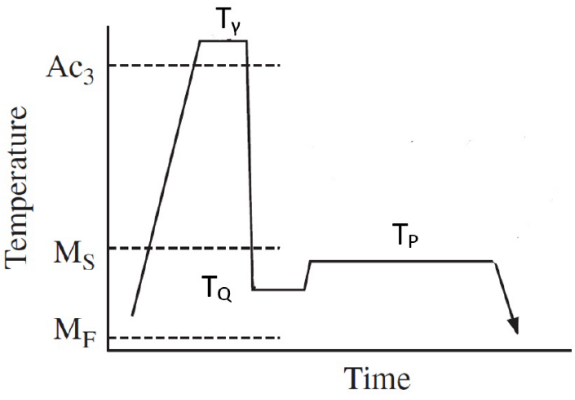

Figure 2.1: Schematic heat-treatment diagram of the quenching and partitioning (Q&P) process [8].

It is essential to understand the carbon partitioning for the development Q&P process. A model has been developed to describe the endpoint of carbon partitioning where competing reactions (cementite, or transition carbide precipitation) are eliminated. According to the provided model, carbon diffusion from primary martensite to untransformed austenite should pursue until the carbon potential becomes equal for both phases as seen in Figure 2.2 [10]. Furthermore, the model assumes that the diffusion of carbon from supersaturated martensite to austenite occurs without any migration of interface. The conditions where the interface is immobile and the chemical potential of carbon is uniform in both phases are known as constrained carbon equilibrium (CCE) [11, 12].

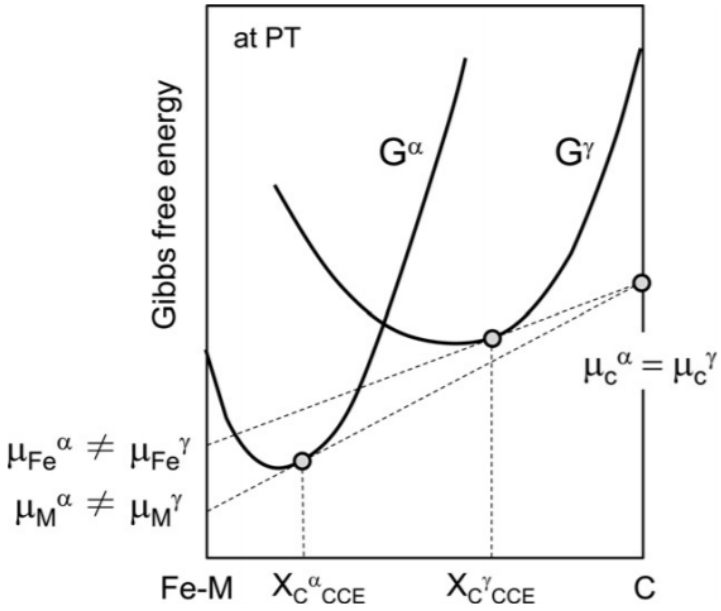

Figure 2.2: Gibbs free-energy vs. composition diagram that satisfies the CCE requirement [10].

In practice, reported volume fractions and carbon content of Q&P treated steels are significantly lower than those predicted by the CCE model due to the carbon consuming competing reactions [4, 5, 10, 13]. Competing reactions during partitioning leave less carbon available for the stabilization of austenite. Therefore, it is essential to minimize the competing reactions to stabilize the largest volume fraction of austenite and obtain the highest austenite stability.

2.2. Q&P Process of Stainless Steels

In the automotive industry, the increase in the thickness of components is directly proportional to the mechanical performance, but at the same time proportional to its weight. Developments in AHSS have allowed researchers to reduce the weight of automotive components by decreasing the thickness of the parts [14]. However, the decrease in thickness makes them susceptible to uniform corrosion and the material loss due to the corrosion decreases the integrity of the steel. The corrosion prevention of AHSS can be improved with galvanization treatment, but the galvanization process brings some problems like zinc depletion and environmental pollution. However, stainless steels have great potential in automobile structures. In addition to excellent corrosion performance, stainless steel allows long-term servicing for thinner structures. However, stainless steels are inadequate in their mechanical strength for automotive structures [15]. To find an optimum point between mechanical properties and corrosion resistance, it is essential to apply suitable heat treatments for specific applications. The mechanical properties of stainless steel can be improved with the Q&P process, but the corrosion behaviour is still a problem due to the combination of different microstructural features. The effect of microstructure on the corrosion performance of Q&P treated stainless steel will be explained in the following sections. This section will provide information about the application of the Q&P process to stainless steel.

The application of the Q&P process to stainless steel has been studied extensively by several researchers to improve the mechanical properties [4, 10]. The main aim of the Q&P treatment is to provide strength and ductility at the same time compared to other heat treatment techniques. In a particular work, the effect of Q&P processing on the mechanical performance was compared with Q&T martensitic stainless steel (AISI 410). The application of the Q&P process improves the strength and ductility balance compared to Q&T steel as seen in Figure 2.3 [4]. The improved work hardening rate in Q&P steel is related to retained austenite. The retained austenite can transform to martensite via TRIP effect under strain. In this particular study, the Q&P steel contained 15 vol% retained austenite and with increasing strain, the reduction in retained austenite volume fraction via TRIP effect is observed with XRD measurements.

Most of the studies related to the Q&P process aim to maximize the retained austenite volume fraction but many researchers have reported that the highest retained austenite fraction is not directly related to superior mechanical properties. The application of the Q&P process to AISI 420 martensitic stainless steel was studied and the optimum combination between strength and ductility was achieved by quenching to 80 °C (353 K) and partitioning at 450 °C (723 K) for 3 minutes as seen in Figure 2.4. In these conditions, 19 vol% retained austenite with the tensile strength of 1570 MPa and total elongation of 15.7% was obtained. However, the highest volume fraction of retained austenite (34 vol%) was obtained with a higher quenching temperature (140 °C - 413 K), but this resulted in lower stability of austenite and inferior mechanical properties [3]. This demonstrates that the mechanical properties of Q&P steels do not only depend on retained austenite fraction, retained austenite stability is also essential for mechanical properties.

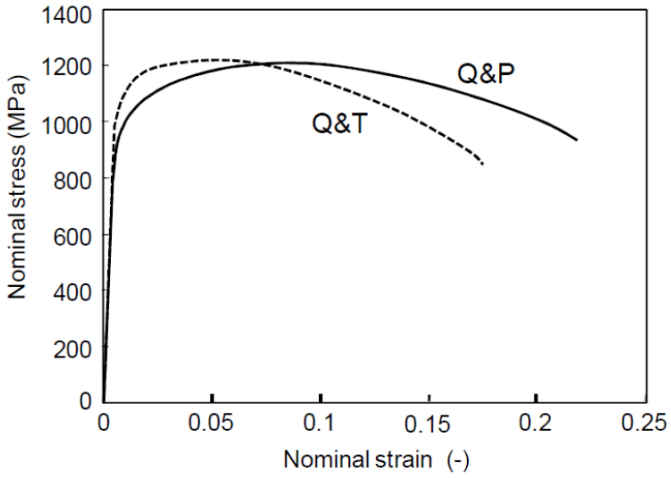

Figure 2.3: Nominal stress-strain curve of AISI 410 steels after Q&P and Q&T treatment [4].

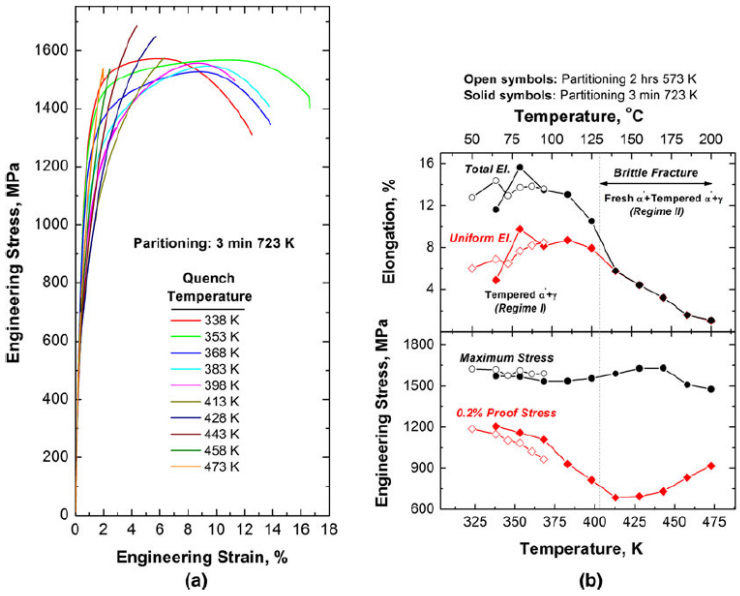

Figure 2.4: Room temperature stress-strain curves for Q&P treated stainless steels partitioned at 723 K (450 °C). (b) Summarized tensile properties of Q&P specimens partitioned at 723 K (450 °C) and 573 K (300 °C) [3].

The stability of the retained austenite can be affected by competing reactions during partitioning. These reactions leave less carbon available for the stabilization of austenite. It is essential to minimize the competing reactions such as carbide precipitation or austenite decomposition to obtain the highest retained austenite stability. From a corrosion point of view, a microstructure free of chromium-rich carbides is better for martensitic stainless steels because the amount of chromium in the matrix remains higher which is essential for passive film formation. The precipitation of chromium-rich carbides is unlikely to form at temperatures below 480 °C due to the limited diffusion of chromium. Therefore, as a partitioning temperature 450 °C is often used because this temperature is low enough to suppress the formation of chromium carbides and at the same time high enough to allow the carbon partitioning to austenite in a short time range [4, 5, 10]. However, the formation of transition carbides and M_3C carbides is possible during the Q&P treatment of martensitic stainless steels. Tsuchiyama et al. [10] reported the precipitation of M_3C carbides (paraequilibrium cementite) in the martensitic regions of Q&P treated martensitic stainless steel (AISI 410) after partitioning at 450 °C for 10 minutes as seen in Figure 2.5 [10].

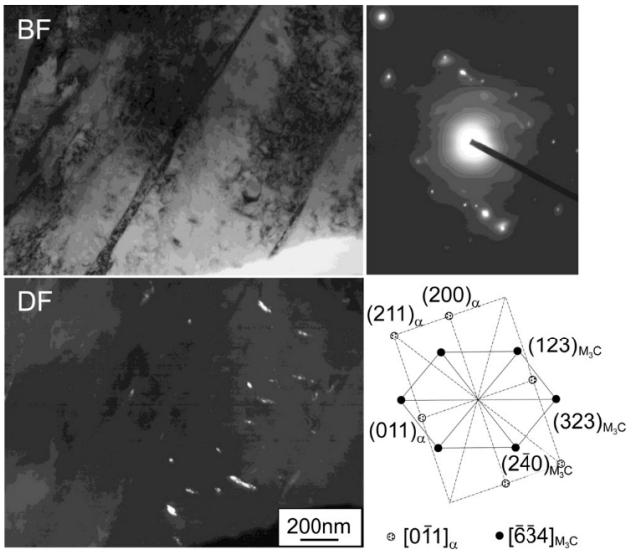

Figure 2.5: TEM images and diffraction pattern for the 450 °C - 10 minutes partitioned martensitic stainless steel [10].

The precipitation of carbides as a competing reaction can lower the stability of the retained austenite. For instance, the cementite precipitation in Q&P steel can be hindered by the addition of silicon due to its low solubility in cementite. In the Q&P process, the mobility of substitutional atoms is limited, and silicon is trapped in cementite during its growth. As a result, the addition of silicon retards the growth kinetics of cementite and suppresses the precipitation of cementite. However, in stainless steel, the presence of chromium can also hinder the precipitation of cementite. Therefore, the need for silicon in Q&P steels has been investigated by many researchers [5, 16]. Tobata et al. [5] studied the Q&P treatment of low carbon martensitic stainless steel. In this study, they found that the addition of silicon to the martensitic stainless steels leads to a retardation of cementite formation. Consequently, the thermal stability and the amount of retained austenite increased.

In addition to silicon, manganese as an austenite stabilizer element is often added to Q&P steels to stabilize the austenite. In general, austenite stabilizers (Ni, Mn) hinder the ferrite to austenite phase transformation by lowering the Ae_1 and Ae_3 temperatures [6].

2.3. Corrosion

Corrosion is the result of an interaction between a metal and the environment which results in degradation. Q&P treated steels can provide significant mechanical properties as a result of multi-phase microstructure. However, the creation of a multi-phase microstructure can affect the electrochemical properties. For this reason, a focus on corrosion and passivation behaviour for Q&P treated martensitic stainless steels is needed.

2.4. Corrosion Electrochemistry

For the corrosion to take place, there must be a formation of corrosion cell and that consists of an anode, a cathode, a metallic path, and an electrolyte.

- Anode: In a corrosion cell, the anode represents the negative terminal of the cell where oxidation takes place. The anode is the reactive metal in the cell and electrons are released at the anode and can move through the cathode.
- Cathode: In a corrosion cell, the cathode represents the positive terminal of the cell. The reduction takes place at the cathode and the electrons from the anode are consumed at the cathode.
- Metallic Path: The electrodes are connected with a metallic conductor (path) and the current flow from cathode to anode through the external metallic path.
- Electrolyte: An electrolyte is an ionic conductor solution for corrosion to occur.

Electrochemical corrosion takes between due to the difference in the electrochemical potential between electrodes. This potential difference between electrodes creates anodic and cathodic areas on the electrode surfaces. The electrons are released at the anodic region and received by cathodic areas to ensure the charge electroneutrality. At the interface between electrode and electrolyte, an electrical double layer is formed, and the electrochemical corrosion process is controlled by the properties of the double layer and the mass transport through the double layer. To deeply understand the electrochemical corrosion mechanism it is essential to understand the thermodynamics and kinetics of the electrode-electrolyte system.

2.5. Thermodynamics

The thermodynamics of the corrosion does provide information about the corrosion tendency of the metals. Consider two different connected metals with different electrochemical potentials. In theory, the metal with the more negative potential will be the anode of the cell and it will dissolve. The main reason behind it is related to the Gibbs free energy and the Gibbs free energy decreases during corrosion that causes spontaneous reactions.

$$G = H + TS \tag{2.1}$$

$$\Delta G = nF\Delta E \tag{2.2}$$

In Eq. 2.1, G is Gibbs free energy, H is enthalpy, S is entropy. In Eq. 2.2, n is the number of charges involved in a reaction, F is Faraday's constant and E is electromotive force. The electromotive force difference in a galvanic couple (a corrosive cell with two different metals separated by an electrolyte) is the driving force for corrosion.

Nernst Equation and Pourbaix Diagrams

The concentration of reducing and oxidizing species can change the electrochemical potential of the cell. For non-standard conditions, the Nernst equation is used to correlate the electrochemical potential of a reaction with the standard electrode potential.

$$E = E^0 - \frac{RT}{nF} \ln\left(\frac{C_{Red}}{C_{Ox}}\right) \tag{2.3}$$

In Eq. 2.3, R is gas constant, C_{Red} and C_{Ox} reduced and oxidised bulk species concentrations. The Nernst equation links the electrode potential with the bulk concentration of species.

The Nernst equation can be used to create Pourbaix diagrams to show the stability of a metal as a function of pH and potential. Pourbaix diagram for iron can be seen in Figure 2.6 [17]. In the active zone of the Pourbaix diagram, iron oxidizes into iron ions. In the passive zone, iron oxides are thermodynamically stable and in the immune zone, the metal is thermodynamically stable which represents the corrosion-free region.

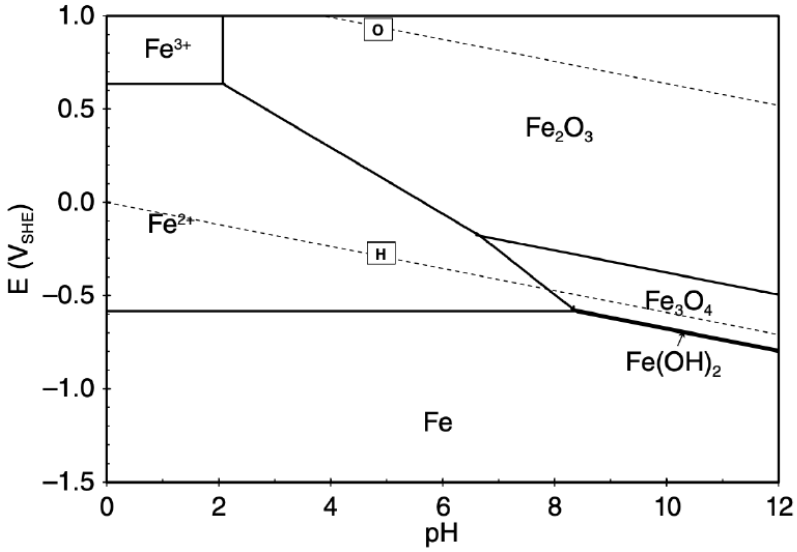

Figure 2.6: Pourbaix diagram for $Fe - H_2O$ system at 25 °C [17].

2.6. Kinetics

Thermodynamics gives an idea about the tendency of electrode reactions to occur. The electrode kinetics addresses the rates of corrosion reactions in the light of Faraday's law. The relationship between an applied current and the amount of product formed can be explained with Faraday's law.

$$v = \frac{j}{nF} \tag{2.4}$$

In Eq. 2.4, v is the reaction rate of species, j is current density, n is number of electrons involved in the process and F is Faraday's constant. The amount of species that are produced or consumed is related to the amount of charge, and hence it is related to the current that passes through the system.

Consider an electrode that is immersed in an electrolyte, at the interface of the electrode there will be a charge transfer. This charge transfer will continue until the electrochemical potentials become equal at both sides of the interface. At the equilibrium potential E_{eq}, oxidation and reduction reactions balance each other out, resulting in zero net currents. In that case, the difference between anodic and cathodic current gives the net current density j.

$$j = |j_{anodic}| - |j_{cathodic}| = 0 \tag{2.5}$$

The current that flows through the interface as anodic or cathodic current is the exchange current density j_0 when the net current is zero.

$$j_0 = |j_{anodic}| = |j_{cathodic}| \tag{2.6}$$

The exchange current density is an essential parameter to control the corrosion rate but since it is an intrinsic property, it is not easy to determine it. To determine the exchange current density, by polarizing the electrochemical system with an external potential to induce some net current in the system. The difference between the applied potential E and the equilibrium potential E_{eq} is known as the overpotential η.

$$\eta = E - E_{eq} \tag{2.7}$$

The application of external current allows controlling the anodic or cathodic net current and through this overpotential-current relationship, it is possible to understand electrode kinetics via the famous Butler-Volmer equation (Eq. 2.8).

$$j = j_0 \left\{ e^{\frac{\alpha_a n F \eta}{RT}} - e^{-\frac{\alpha_c n F \eta}{RT}} \right\} \tag{2.8}$$

Butler-Volmer equation is a fundamental relationship for electrode kinetics. In this equation, the exchange current density corresponds to the corrosion current density, which is used to calculate the corrosion rate from Eq. 2.9, where a is molar mass and ρ is the density.

$$r = \frac{a j_0}{\rho n F} \tag{2.9}$$

2.7. Pitting Corrosion

Corrosion may not have a detrimental effect on a metal immediately but it affects the mechanical properties or the appearance. In order to select suitable materials for engineering applications, it is essential to understand the types of corrosion. This section will provide information about pitting corrosion which is an important type of corrosion for stainless steel.

Pitting corrosion is a localized form of corrosion and metal surfaces corrode preferentially by forming pits or cavities. Especially, metals which form passive films are more susceptible to pitting corrosion (the breakdown of a passive film leading to the dissolution at localized sites). It is the most dangerous form of corrosion because it is hard to predict the formation of pits and detect them [18]. In particular, pitting corrosion is an important type of corrosion for stainless steel, and it is one of the focus areas of this thesis.

In mild corrosive environments, stainless steels exhibit sufficient corrosion performance due to the formation of a passive film on the surface. The localized dissolution of the passive layer is one of the major sources of pitting corrosion. The stochastic dissolution of the passive film generates microscopic holes on the metal surface and the size of the holes increases with the aggressiveness of the corrosive medium. As a nature of pitting corrosion, particular microscopic pits are anode while remaining portions of the steel surface remain passive and cathodic [19].

The pitting corrosion mechanism generally consists of pit initiation and pit propagation stages. The pit initiation stage is the product of the electrochemical action of ions at specific regions (heterogeneities) in the oxide layer. Once a pit nucleates, pit propagation proceeds autocatalytically, and this autocatalytic reaction produces cavities on the surface. In particular, chloride rich environments deteriorates the oxide film and at preferential sites accelerate the formation of pits. The presence of chloride ions in pits stimulates the redox reactions necessary for the propagation of the pits. The pit propagation involves the anodic dissolution of metallic and chloride ions within the pits. The diffusion of metallic cations into the pit causes the chloride concentration within the pit to increase resulting in accelerated propagation of the pitting corrosion. This phenomenon hinders the repassivation of the steel which otherwise will hinder the pit propagation [20, 21]. In addition to pitting corrosion, crevice corrosion is a localized form of corrosion too and caused by the deposition of deposits on a metal surface or by the presence of gaps or cavities between adjacent surfaces [18].

In particular, a stainless steel microstructure free of chromium-rich carbides is desirable because the chromium level of the matrix will remain higher in the absence of carbides. As mentioned above, the pits initiate at heterogeneities in the passive film and the initiation of the pit is followed by the breakdown of the passive layer which deteriorates the corrosion resistance. As a result, in stainless steel, the presence of chromium-rich carbides are preferential sites for the formation of pits to deteriorate the corrosion performance [21].

2.8. Corrosion Behaviour of Q&P Stainless Steels

Martensitic stainless steel is widely used in vehicle production, power plants and building structures to provide strength and toughness combination with moderate corrosion performance [22]. The martensitic microstructure in martensitic stainless steel is produced by a Q&T route. The martensitic stainless steel is annealed at an austenitization temperature of 950-1050 °C and followed by quenching. The application of different heat treatment parameters (austenitizing temperature, holding time, heating rate, cooling rate) can affect the mechanical properties [23]. The martensitic stainless steel in the quenched state is quite hard and brittle and not suitable for engineering applications. The application of tempering treatment with suitable tempering parameters can improve the mechanical properties of martensitic stainless steel. On the other hand, inappropriate tempering conditions can lead to the formation of chromium-rich carbides in the vicinity of grain boundaries and martensite laths. These carbides typically nucleating from M_3C to M_7C_3 and then transforms to $M_{23}C_6$ [24–27].

The corrosion properties of Q&T martensitic stainless steel have been studied extensively [22, 24, 28]. However, only a little research can be found in the literature about the corrosion behaviour of Q&P treated steels, especially Q&P treated martensitic stainless steels.

The corrosion behaviour of a Q&P treated medium carbon steel in NaCl was investigated by Yang et al. [29]. In this work, the Q&P specimen exhibits a lower corrosion rate compared to the Q&T steel. The reason for the lower corrosion rate in Q&P steel is related to the formation of carbon-rich retained austenite and the carbon depleted martensite. The carbon-rich retained austenite increases the corrosion potential and the carbon depleted martensite decreases the residual tensile stresses.

Mehner et al. [30] studied corrosion performance of low alloy Q&P steels and same low alloy Q&T steel by using electrochemical impedance spectroscopy. In the Q&T process, carbon is dissolved in martensite and alter the potential to be more cathodic. In tempering, carbon atoms in martensite diffuse into austenite, making carbon depleted martensite zones anodic. As a result, these zones become more anodic compared to the rest of the microstructure. In the Q&P process, the diffusion of carbon from super-saturated martensite to the austenite makes it martensite anodic compared to the austenite. The total cathodic area for the Q&P steel is smaller than the Q&T steel as illustrated in Figure 2.7. Thus, the corrosion rate for Q&T steel becomes significantly higher than Q&P steel.

Dieck et al. [31] studied the corrosion behaviour of Q&P treated martensitic stainless steels and compared it with the same Q&T steel by using electrochemical potentiodynamic reactivation (EPR). They found that Q&P steels exhibit better corrosion performance compared to Q&T steel. In Q&T steel, the formation of chromium-rich carbides creates a chromium depleted zone in the microstructure. From the EPR test of Q&T steel, it is possible to observe an increment in the current densities during activation and re-activation of the passivation layer. However, in Q&P treated martensitic stainless steels no chromium depletion was detected, and for all partitioning times, a stable passivation layer is observed.

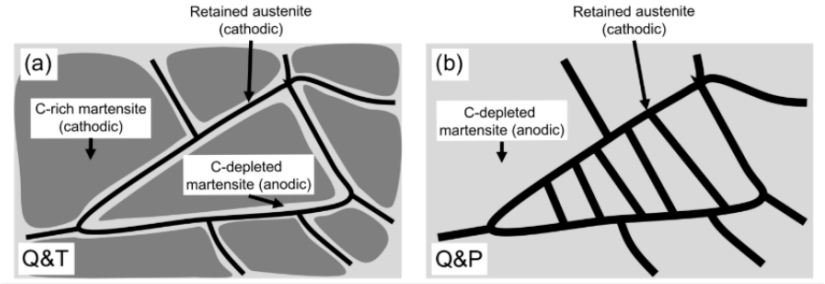

Figure 2.7: Schematic representing the microstructure of (a) Q&T and (b) Q&P structures [30].

Lu et al. [32] studied corrosion performance of martensitic stainless steel in Q&P and Q&T forms. In this study, for specific partitioning temperatures, the pitting potential was improved. The Q&P treatment reduces the pitting susceptibility of martensitic stainless steel when they are partitioned at 350 °C and 450 °C. Through the Q&P process, the formation of chromium-rich carbides is prevented, and a sufficient amount of retained austenite is obtained at the end of the process. Therefore, it is possible to observe better pitting resistance in Q&P treated steel compared to Q&T.

In conclusion, Q&P treated martensitic stainless steel exhibit better corrosion performance compared to the Q&T treated martensitic stainless steel. The presence of carbides in Q&T steel microstructure deteriorate the corrosion performance since they act as a pitting initiation site. On the other hand, it is not possible to observe plenty of carbides in Q&P treated martensitic stainless steels and they are not detrimental as in Q&T martensitic stainless steels. In Q&P treated martensitic stainless steels, the carbon-rich retained austenite and carbon-depleted primary martensite can play a positive role together to reduce the corrosion rate. Retained austenite is a soft phase, thus easily tolerating the shape change caused by the martensitic transformation, further relaxation of internal stresses in retained austenite decreases the corrosion rate. In addition to retained austenite, the primary martensite decreases its lattice distortions via carbon depletion. As a result, the primary martensite becomes soft, which reduces the free energy and increases the corrosion potential. Considering the potential applications of Q&P treated steels, there is a need for a detailed investigation of the effect of microstructure on the corrosion behaviour of Q&P treated martensitic stainless steels.

2.9. Passivation and Oxide Film Properties

An oxide layer starts to develop on the surface of the metal when corrosive species oxidize the surface. The protective passive oxide layer can limit corrosion by diminishing ion and/or electron transfer.

For corrosion protection, the structure, composition and semiconducting behaviour of the oxide layer are essential. In addition, compactness of the oxide layer is one of the critical factors that determine corrosion protection, irregular and/or porous structures allow corrosive species to penetrate through the metal under the protective oxide film [33].

The composition and the semiconducting property of the passive film vary with alloy composition and the pH of the electrolyte. The main effect of an increasing pH on film formation is a thickening of the passive film. In alkaline solutions, iron oxide is more stable. Thus, an increase in the amount of Fe (III) oxide is observed on the passive film of Fe-Cr alloys in an alkaline medium. Conversely, in acidic solutions, a chromium oxide film is more stable on the passive film of Fe-Cr alloys due to the slower dissolution of chromium oxide [34].

Concerning the semiconductive behaviour of the passive films of stainless steel, it has been proposed that films formed in neutral to alkaline pH are composed of a chromium-rich inner layer (p-type semiconductor), and an iron-rich outer layer (n-type semiconductor) [35]. Depending on the predominant defects in the passivation layer of stainless steels, either p-type and/or n-type behaviour can be observed. The passive films rich with cation vacancies generally behave as p-type. On the other hand, in n-type behaviour, cation interstitials and/or anion (oxygen ion) vacancies act as electron donors in the passive film of stainless steel. However, it is not possible to separate the contribution of anion vacancies (oxygen vacancies) and cation interstitials. [36].

The passive films properties that formed on stainless steel are impacted by several microstructural features. These features are grain boundaries, chemical composition, galvanic coupling between microstructural features, residual stresses, and so on. For instance, grain boundary structure controls the corrosion behaviour in both grain scale and sub-grain scale. In grain scale, the size and/or morphology of the grains can influence the corrosion performance, in sub-grain scale, the presence of dislocations can affect the corrosion performance by controlling the residual stresses. In general, smaller (acicular) grains increase the surface activity with excessive residual stresses which deteriorate the corrosion resistance [37]. In addition, the presence of residual stress creates more active microstructures, for instance, martensitic transformation generates residual stresses due to the change in crystal structure and the distorted structure deteriorates the corrosion performance [38]. Also, carbon diffusion to dislocation rich zones on the surface creates local cathodic zones which accelerate the effect of galvanic coupling by increasing the cathodic area [30].

The effect of grain size reduction on the passive film properties of ferritic stainless steel was investigated, and it was reported that the grain refinement deteriorates the film properties and the deterioration can be explained by the increase in both acceptor and donor density with grain size reduction [39].

The effect of grain refinement on the passive film properties of austenitic stainless steel was studied in a borate buffer chloride-containing solution, and it was reported that the pitting potential and barrier properties are worsening with grain refinement [40].

The grain size effect on the passive film properties was studied by comparing ultra-fine grained, fine-grained and coarse-grained austenitic stainless steel in NaCl medium. Due to the formation of more stable film in ultra-fine grained samples, they exhibit better corrosion performance compared to the fine and coarse-grained samples. The lowest corrosion resistance belongs to coarse-grained austenitic stainless steel sample [41].

The effect of grain size reduction on the passive film properties of ferritic stainless steel was investigated, and it was reported that the passive film formed on the fine-grained sample was less defective than that of the coarse-grained. In other words, the number of point defects was decreased with grain refinement [42].

According to the literature, it is possible to find contradictory results on the relationship between grain size and passive layer properties of stainless steel. In addition to grain size, the passive layer properties of stainless steels can be affected by microstructural features. One of the aims of this master thesis is to create a connection between microstructural features and the passivity behaviour of Q&P treated martensitic stainless steels by combining Mott-Schottky analysis with X-ray photoelectron spectroscopy (XPS).

2.10. Research Approach and Thesis Focus

The mechanical behaviour of the Q&P treated martensitic stainless steels have been investigated deeply to combine the strength of the martensite with the ductility of the retained austenite. Unlike mechanical behaviour, the corrosion behaviour of Q&P treated martensitic stainless steel has not been investigated in depth. The effect of environmental factors or the effect of microstructure on the corrosion performance of Q&P martensitic stainless steel needs to be studied. This thesis aims to create a connection between the microstructural features and the corrosion behaviour of Q&P treated martensitic stainless steels. In particular, in this work, the effect of retained austenite on the corrosion and passivation behaviour of the Q&P treated martensitic stainless steels were investigated. As an experimental path, potentiostatic polarization, open circuit potential (OCP), electrochemical impedance spectroscopy (EIS), potentiodynamic polarization were performed in 3.5 wt.% NaCl to investigate the corrosion response of Q&P treated martensitic stainless steels and Mott-Schottky experiments were carried out in 3.5 wt.% NaCl solution to reveal the passive film properties of the Q&P treated martensitic stainless steels. In addition, X-ray photoelectron spectroscopy (XPS) was performed to analyze the chemical composition and fractions of oxide layers in the passive film.

3

Experimental Procedure

To analyse the effect of microstructure on the corrosion behaviour of Q&P treated martensitic stainless steels, it is essential to understand the corrosion response of individual microstructural features and their interactions.

For this investigation, series of alloys with a Q&P microstructure is created (the microstructural development part is taken from the Master Thesis of Benne de Bakker). After the microstructure creation, electrochemical experiments were performed to explore the corrosion and passivation behaviour of these steels. The experimental details and the microstructure development are explained in this section.

3.1. Microstructure Characterization

3.1.1. Material

A new stainless steel composition was designed considering a target microstructure of tempered martensite and retained austenite after Q&P processing. The chemical composition of Q&P processed steel is presented in Table 3.1. The selected composition for the Q&P process was cast using vacuum induction melting by Acerinox. Then, cast ingots were homogenized for 3 hours at 1270 °C. The ingots were hot rolled into slabs by RINA-CSM. Then, each slab was slowly cooled to room temperature. Lastly, all plates were annealed for 24 hours at 600 °C [43].

Table 3.1: Chemical composition (wt.%) of Q&P treated steel sample.

Alloy	C	Si	Cr	Mn	Fe
Q&P	0.2	0.35	12.5	0.7	bal.

3.1.2. Design of the Q&P Treatment

Thermodynamic calculations were performed with Thermo-Calc Software before the experimental procedure to predict the phase stabilities and critical temperatures. The complete dissolution of $M_{23}C_6$ carbides occurs above 950 °C as seen in Figure 3.1. The phases that are relevant to this study is ferrite (BCC_A2#3), austenite (FCC_A1#3)) and chromium-rich carbides (M23C6).

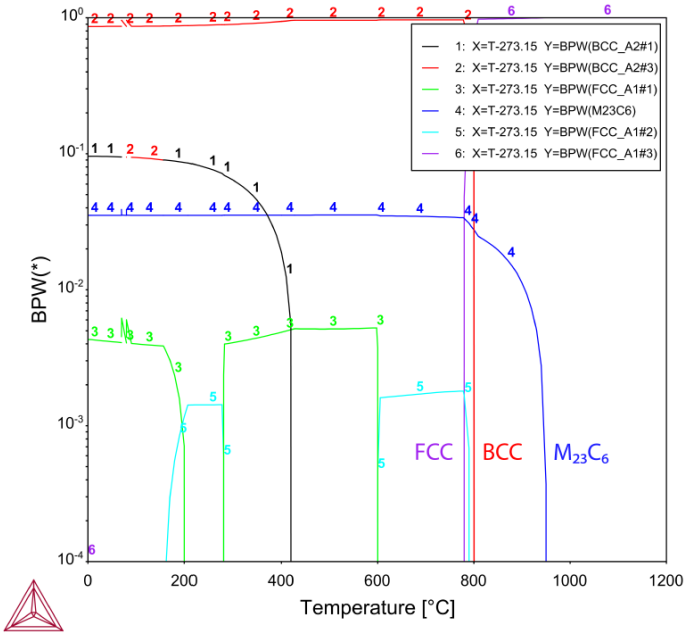

Figure 3.1: Phase mass fraction (BPW(*)) vs. temperature graph for the studied alloy [43].

In addition to Thermo-Calc, to predict the critical temperatures, an empirical approach was used to calculate the martensite-start temperature of the alloy. From the literature, the experimental data for the Q&P process of 13Cr martensitic stainless steel resulted in the following equation.

$$M_S\,(^\circ C) = 553.7 - 530.8w_C - 9.7w_{Si} - 12.1w_{Cr} - 30.4w_{Mn} \tag{3.1}$$

In Eq. 3.1, w_i represents the concentration of the elements in weight percent. The coefficients for Mn and Cr are taken from the well-known Andrews equation [44] which was validated by Kung and Rayment [45] for steels with up to 12 wt% Cr and 5 wt% Mn. The M_s temperature for the studied alloy is calculated as 272 °C.

Several experiments were performed to determine suitable processing parameters for the Q&P treatment of the alloy. In this section, a detailed explanation of the experimental procedure is given by considering the selection of heat treatment conditions.

Selection of Austenitizing Conditions

The austenitizing conditions are essential for the Q&P treatment. The stability of austenite during partitioning depends on the availability of carbon in austenite. The carbon has to dissolve completely during the austenitization stage. In martensitic stainless steel, the main aim of this stage is to dissolve chromium-rich carbides such as $M_{23}C_6$.

The dissolution of chromium-rich carbides during austenitizing raises the concentration of carbon and chromium in solid solution which decreases the M_s temperature. This reduction in M_s temperature with austenitizing conditions has been studied extensively in martensitic stainless steel [13, 16, 46, 47]. However, the austenitizing temperature to dissolve chromium-rich carbides can vary in literature from 1000 °C (30 minutes) [10] to 1250 °C (2 minutes) [13].

In general, a higher austenitizing temperature has a greater effect on accomplishing complete austenitization and dissolution of carbides than longer hold times at some lower temperatures. However, 1100 °C (15 minutes) was used as an austenitizing temperature due to some limitations in the dilatometry measurement.

Selection of Cooling Rate Conditions

The cooling rate is important to achieve desired microstructural features. The cooling rate from austenitizing needs to be high enough to avoid ferrite and pearlite formation. For the selection of the suitable cooling rate, samples were subjected to several dilatometry experiments. All samples were austenitized at 1100 °C for 15 minutes and cooled to room temperature with a cooling rate of 1 °C/s, 5 °C/s, 10 °C/s, 20 °C/s.

As a result, it was decided to use a cooling rate of 5 °C/s for all Q&P treatments. This cooling rate is low enough to allow for precise control of the quenching stage and high enough to prevent competing/side reactions during cooling.

Martensite Kinetics

The martensite transformation kinetic is an essential parameter for the Q&P process. The Koistinen-Marburger relationship is used to describe the progress of martensitic transformation. The Koistinen-Marburger relationship combines the extent of the martensitic transformation with an undercooling. In the following Koinstinen-Marburger expression where f_M is the fraction of primary martensite, M_s for martensite start temperature and QT for quenching temperature [48].

$$f_M = 1 - \exp\left[-\alpha_m \cdot (M_S - QT)\right] \qquad M_S > QT > -80°\text{C} \tag{3.2}$$

The transformation rate parameter (α_m) is usually a constant value and independent of composition. However, several researchers have suggested that the transformation rate parameter can vary with chemical composition, the rate parameter was calculated based on an empirical equation [49].

$$\alpha_m \left(K^{-1}\right) = 0.0224 - 0.0107 w_C - 0.0007 w_{Mn} - 0.00005 w_{Ni} - 0.00012 w_{Cr} - 0.0001 w_{Mo} \quad (3.3)$$

From Eq. 3.3, the transformation rate parameter (α_m) was calculated as 0.0183 for the studied alloy.

In addition to the Koistinen-Marburger model, the martensitic transformation was investigated experimentally. The relative change in length was measured by dilatometry and the relationship between temperature and martensite fraction is estimated by using the lever rule [43].

Selection of Quenching Temperatures

The Koistinen-Marburger can be used to select the suitable quenching temperature and to calculate the untransformed austenite fraction [50]. In this work, the volume fraction of untransformed austenite was calculated by using Eq. 3.1, Eq. 3.3 and Koistinen-Marburger relation. From these equations, the untransformed retained austenite fraction for selected quenching temperatures is shown in Table 3.2 [43].

Selection of Partitioning Conditions

In this work, initial quenching followed with a partitioning at 450 °C for 5 minutes with a heating rate of 10 °C/s. The partitioning conditions were selected from the literature [3, 4, 13]. At 450 °C, the precipitation of chromium-rich carbides is unlikely to form during the partitioning step [3].

Table 3.2: Selected quenching temperatures and untransformed austenite fractions [43].

Sample ID	Quenching Temperature (°C)	Untransformed austenite fraction at QT
QT113	113	0.10
QT155	155	0.20
QT183	183	0.30
QT205	205	0.40
QT220	220	0.50

3.1.3. Dilatometry

The heat treatments were performed using a dilatometer. Dilatometry is a device to study solid-state phase transformations because it allows for monitoring the change in length as a function of temperature and time. From the change in length in the sample as a function of temperature, it is possible to evaluate phase transformation and transformation temperatures.

The heat treatments were designed to produce several Q&P microstructures. The overall heat treatment presented in Figure 3.2 with the following treatment parameters:

- Full austenitization of the initial microstructure at 1100 °C for 15 minutes with a heating rate of 10 °C/s.
- Cooling rate of 5 °C/s for cooling to quenching temperature.
- Holding time at quenching temperature of 20 seconds followed with a partitioning at 450 °C for 5 minutes.
- Cooling rate of 5 °C/s for cooling to room temperature after partitioning to complete the heat treatment.

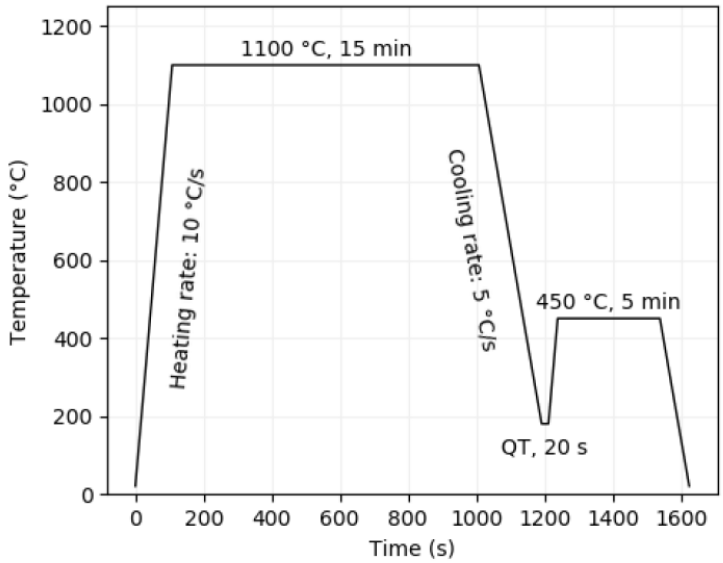

Figure 3.2: Overview of the Q&P heat treatment used in this study [43].

The Q&P microstructure was generated through several types of heat treatments. All specimens were heated at 10 °C/s to an austenitizing temperature of 1100 °C. After holding for 15 minutes, the specimens were cooled to specific quenching temperatures between M_s and M_f temperatures with a cooling rate of 5 °C/s. Initial quenching followed with a partitioning at 450 °C for 5 minutes. Then to complete the Q&P treatment all samples quench to room temperature with a cooling rate of 5 °C/s.

3.1.4. Sample Preparation

The microstructures obtained from different Q&P treatments were prepared for optical microscopy examinations. The samples were first embedded in a hot mounting machine. After the mounting, the samples were ground with sanding paper from 320 to 4000 grit. All samples were polished using a diamond suspension with 3 and 1 µm particle sizes. For the microstructural analysis, few samples were etched (20 to 30 seconds) with a Vilella's reagent to reveal the microstructural details.

3.1.5. Investigation of the Microstructure

The final microstructures of different Q&P treatments were analyzed with optical microscopy. A Keyence VHX-500 optical microscope was used to characterize the overall microstructure.

3.2. Electrochemical Analysis

Electrochemical analysis was performed for 6 different samples. Out of these 6 samples, 5 of them are Q&P treated martensitic stainless steel. One of them is an annealed commercial martensitic stainless steel (AISI 420) with a chemical composition (wt.%) of 0.4 C, 0.35 Si, 14 Cr, 0.7 Mn and (Bal.) Fe.

3.2.1. Sample Preparation

The samples were ground with sanding paper from 320 to 4000 grit. After that, all samples were polished using a diamond suspension with 3 and 1 µm particle sizes to obtain a proper surface for electrochemical experiments. The edge of the samples was coated with a lacquer to prevent them from crevice corrosion. In addition, the bottom side of the sample is ground to create a working electrode contact for the electrochemical cell. The sample preparation steps were repeated for all electrochemical tests. An example of a sample for an electrochemical test is shown in Figure 3.3.

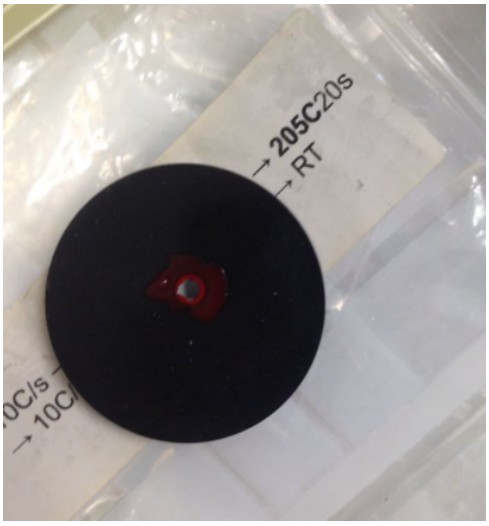

Figure 3.3: An example of the completed sample for electrochemical experiments.

3.2.2. Electrochemical Setup

A Biologic VSP-300 potentiostat was used in combination with a three-electrode electrochemical cell setup for the experiments. In the setup, platinum mesh as the counter electrode, the sample as the working electrode and Ag/AgCl (saturated KCl) as the reference electrode were used. EC-Lab v11.36 software was used to control and analyze the electrochemical measurements. The electrochemical cell setup was placed in a cage to shield it from external noises and all experiments were conducted at room temperature. The electrochemical setup is shown in Figure 3.4.

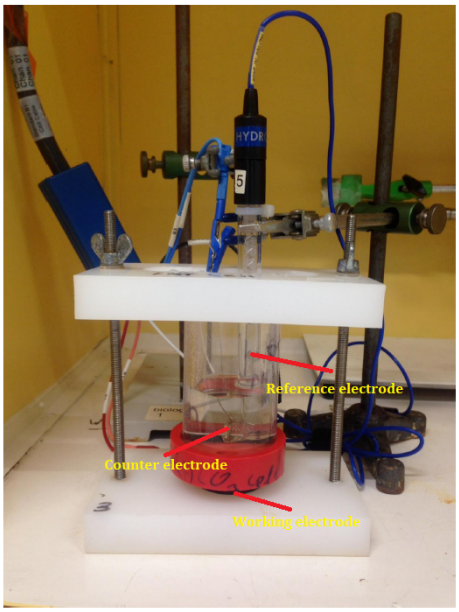

Figure 3.4: Electrochemical cell setup.

3.2.3. Electrochemical Experiments

Electrochemical experiments were carried out in a 3.5 wt.% NaCl (pH 6.7) to assess the role of microstructure on the corrosion behaviour. 3.5 wt.% NaCl solution was used as an electrolyte due to the presence of Cl^- ions in the solution that initiate pitting corrosion by breaking down the protective oxide film.

Corrosion experiments were initiated by cathodic potentiostatic polarization and followed with measuring the open circuit potential, then the corrosion resistance was measured with electrochemical impedance spectroscopy, and finally, the corrosion response of the samples was analysed with potentiodynamic polarization. All tests were repeated at least 3 times to verify the reproducibility of the results.

Cathodic Potentiastatic Polarization

Cathodic potentiastatic polarization was applied to samples to remove the natural oxide layer of martensitic stainless steel and the applied potential was -300 mV (vs. OCP) for 10 minutes.

Open Circuit Potential

Open circuit potential (OCP) of the samples were recorded for 30 minutes relative to the Ag/AgCl reference electrode in 3.5 wt.% NaCl medium to make the system stable.

Electrochemical Impedance Spectroscopy

Electrochemical impedance spectroscopy (EIS) was used to measure the electrochemical responses of the passive layer that formed on Q&P processed martensitic stainless steel samples. EIS measurements were carried out by applying an alternating current (AC) perturbation in the frequency range from 30 kHz to 0.01 Hz with a 10 mV peak-to-peak amplitude after a stable OCP was achieved.

The Zview 4 software is used to fit the experimental EIS data into equivalent electrical circuits.

Potentiodynamic Polarization

Potentiodynamic polarization was conducted to determine the effect of the microstructure on the corrosion response of the stainless steel samples. The samples were polarised in a potential range between -0.3 V to 0.4 V with respect to the OCP with a scan rate of 0.167 mV/s.

Corrosion potential and corrosion current density values were calculated through Tafel slopes from the linear parts of the polarization curves by using EC-Lab v11.36 software.

Mott-Schottky Measurements

Mott-Schottky measurements were performed to study the effect of microstructure on the semiconducting properties of the passive film. The OCP of the samples were recorded for 30 minutes to form a passive layer. Mott-Schottky measurements were carried out by applying an AC perturbation at a fixed frequency of 1 kHz with 10 mV amplitude. A potential range of 0.1 V to -0.3 V (reverse scan) was swept with a step size of 50 mV.

3.3. Passive Layer Analysis

X-ray Photoelectron Spectroscopy

X-ray photoelectron spectroscopy (XPS) measurements were conducted to analyze the chemical composition of different oxide layers in the passive layer of Q&P treated martensitic stainless steels. Before XPS measurements, grinding and polishing steps were repeated to obtain a mirror-like surface. Then, the samples were rinsed with ethanol and dried with compressed air. XPS analysis was carried out using a PHI-TFA XPS spectrometer, equipped with an Mg-monochromatic X-ray source. Narrow multiplex scans of the peaks were recorded using a pass energy of 20 eV with a step size of 0.1 eV, at a take-off angle of 45° with respect to the sample surface. Low energy electron gun was used for surface charge neutralization XPS. The elemental composition was determined from the XPS survey spectra, high-energy resolution spectra of O 1s, C 1s, Fe 2p and Cr 2p photoelectron peaks were curve-fitted by using Multipak v8.0.

4

Results and Discussion

The results from experimental investigations are presented in this section. The corrosion response of the Q&P treated martensitic stainless steels and the passivity behaviour of these steels is discussed and compared with an annealed commercial martensitic stainless steel (AISI 420). In this section, the corrosion response of the samples and the passivity response is discussed considering the microstructural features and their interactions.

4.1. Application of the Q&P Treatment

All samples were subjected to Q&P treatments with varying quenching temperatures. Phase fractions of Q&P processed specimens (the phase fraction values are estimated from the Master Thesis of Benne de Bakker) with different quenching temperatures as shown in Table 4.1 [43] and these Q&P treated martensitic stainless steels were used for electrochemical measurements. For the Q&P treated alloys, the highest retained austenite fraction (0.22) was achieved at a quenching temperature of 183 °C.

Table 4.1: Phase fractions of Q&P processed specimens with different quenching temperatures [43].

Sample ID	Retained austenite fraction	Fresh martensite fraction
QT113	0.06	0.04
QT155	0.18	0.02
QT183	0.22	0.08
QT205	0.18	0.22
QT220	0.12	0.38

4.2. Electrochemical Measurements

The electrochemical experiment results of the Q&P treated martensitic stainless steel and annealed AISI 420 steel is presented in this section. The electrochemical measurement aims to create a relation between the microstructural features and the corrosion behaviour of Q&P treated martensitic stainless steels. As an experimental path, potentiostatic polarization, open circuit potential (OCP), electrochemical impedance spectroscopy (EIS), potentiodynamic polarization and Mott-Schottky experiments were carried out in 3.5 wt.% NaCl solution to reveal the corrosion response and the passive film properties of Q&P treated steels.

Potentiastatic Polarization

Potentiastatic polarization was applied to remove the natural oxide layer of the stainless steels and the applied potential was -300 mV (vs. OCP) for 10 minutes as shown in Figure 4.1. For all samples, after 10 minutes of potentiostatic polarization, the constant current was achieved.

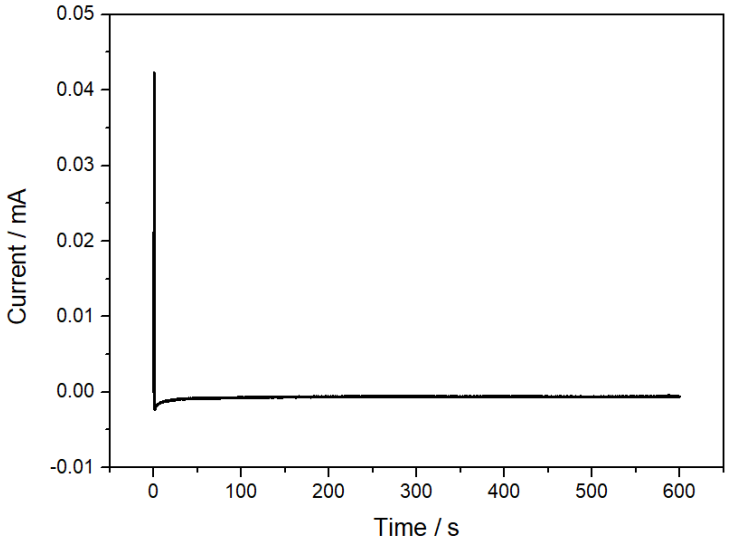

Figure 4.1: Potentiastatic polarization curve at applied potential of -300 mV (vs. OCP) for 10 minutes in 3.5 wt.% NaCl solution.

Open Circuit Potential

Figure 4.2 shows the OCP measurements of all samples in 3.5 wt.% NaCl solution. OCP values have stabilised after 30 minutes. The measurements show a similar trend for both Q&P treated steels and AISI 420. For all samples, the open-circuit potential shifts to more positive values, which is indicative of the passive film formation.

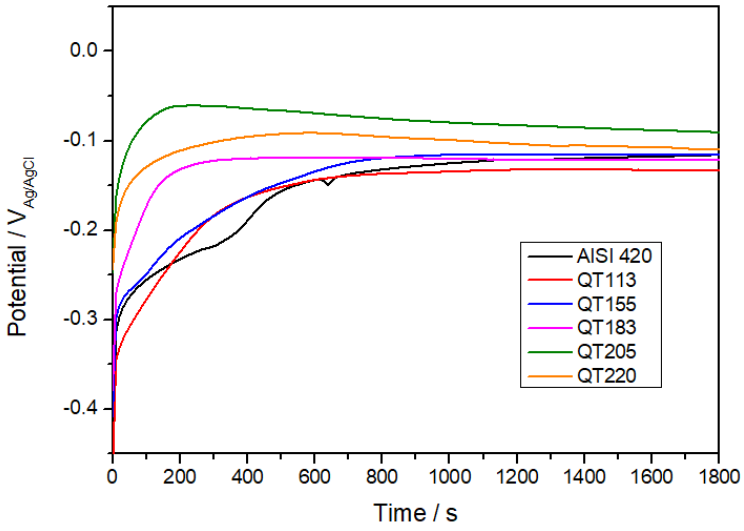

Figure 4.2: The open circuit potentials of commercial martensitic stainless steel (AISI 420) and Q&P treated martensitic stainless steels in 3.5 wt.% NaCl solution.

Potentiodynamic Polarization

Potentiodynamic polarization tests were conducted to measure the corrosion resistance of the steels. Potentiodynamic polarization plots are shown in Figure 4.3. Polarization curves of all stainless steel samples show a clear passivation behaviour which allows analysis of the passivation response of the samples. All Q&P treated martensitic stainless steel samples with different microstructures show similar polarization behaviour in 3.5 wt.% NaCl electrolyte. Table 4.2 summarizes the polarization parameters obtained from the polarization curves by the Tafel extrapolation method.

Table 4.2: Corrosion current density (i_{corr}), corrosion potential (E_{corr}) and pitting potential (E_{pit}) values of Q&P processed and AISI 420 steels calculated from the potentiodynamic polarization experiments.

Sample ID	i_{corr} ($10^{-8} xA/cm^2$)	E_{corr} (mV)	E_{pit} (mV)
AISI 420	5.62 $\pm$ 1.76	-122 $\pm$ 12	127 $\pm$ 20
QT113	4.89 $\pm$ 1.92	-134 $\pm$ 16	92 $\pm$ 19
QT155	4.32 $\pm$ 2.18	-140 $\pm$ 15	130 $\pm$ 29
QT183	3.64 $\pm$ 2.25	-127 $\pm$ 14	200 $\pm$ 42
QT205	4.97 $\pm$ 2.34	-96 $\pm$ 15	259 $\pm$ 12
QT220	5.12 $\pm$ 2.63	-130 $\pm$ 10	146 $\pm$ 42

Results reveal that the AISI 420 steel corrodes slightly faster than the Q&P treated steel. The corrosion current density (i_{corr}) value for the AISI 420 is slightly

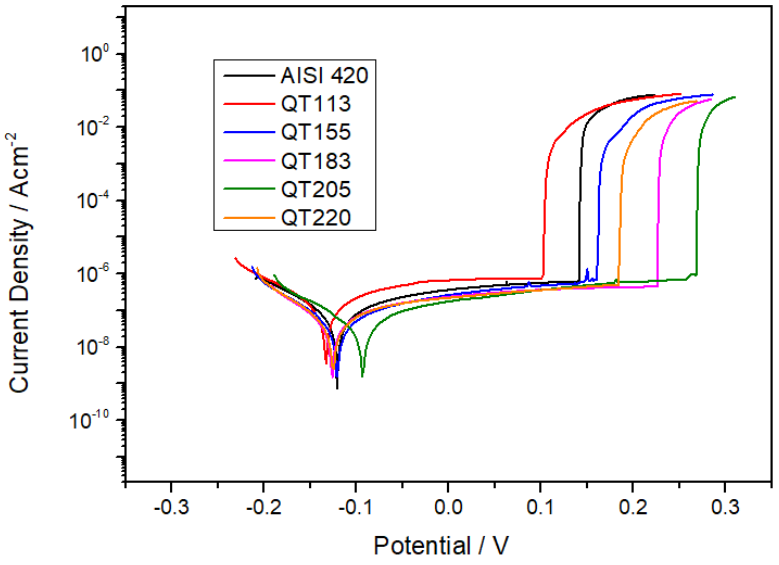

Figure 4.3: Potentiodynamic polarization plots of commercial martensitic stainless steel (AISI 420) and Q&P treated martensitic stainless steels in 3.5 wt.% NaCl solution.

high compared to the Q&P treated martensitic stainless steels. A comparison between corrosion performance of Q&P treated martensitic stainless steels can be done. The lowest corrosion current density belongs to the QT183 steel among all Q&P treated martensitic stainless steels. The current density value for the QT113, QT155 and QT183 steels is lower than the QT205 and QT220 steels. For the QT113, QT155 and QT138 steels, the fresh martensite content is insignificant compared to the QT205 and QT220 samples. The higher corrosion current density for the QT205 and QT220 steels can be correlated with the high amount of fresh martensite.

In addition, pitting potential (E_{pit}) is improved with the Q&P treatment as seen in Figure 4.4. Except for the QT113, all Q&P treated martensitic stainless steels have higher E_{pit} compared to the annealed AISI 420. This behaviour can be explained by the presence of carbides (M_3C, M_7C_3, $M_{23}C_6$) in the microstructure of the annealed AISI 420 [23]. The presence of carbides in the microstructure act as pit initiation sites.

On the other hand, it has been investigated that the corrosion resistance of austenite is higher than ferrite/martensite [21, 51] due to that austenite contains lower residual stress and fewer defects [52]. Therefore, the distribution of the retained austenite might affect the pitting resistance of the Q&P treated martensitic stainless steels [53], the residual stress of the martensitic grain would be released because the less stressed retained austenite, and the localized corrosion performance of the Q&P treated steel will be more resistant.

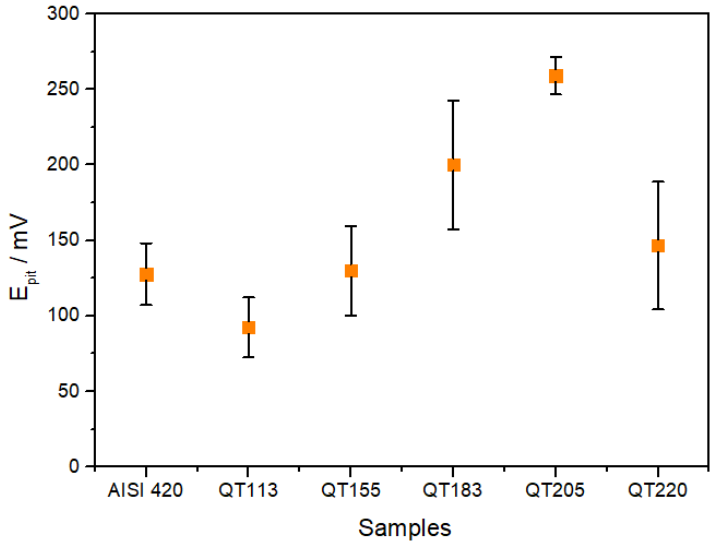

Figure 4.4: Pitting potentials (E_{pit}) of the stainless steel samples based on potentiodynamic polarization curves.

Moreover, passivation current density values for all samples are calculated from the end of the passivation region. The passivation current densities for all steels is shown in Figure 4.5 The passivation current density for both AISI 420 and Q&P treated steels is in the order of $10^{-7}\ A/cm^2$.

Electrochemical Impedance Spectroscopy

Figure 4.6 shows EIS measurement results in the form of a Nyquist plot. Figure 4.7 and 4.8 display EIS measurement results in the form of Bode plots. All curves in the Nyquist plots show similar characteristics of arcs with different diameters. Nyquist plots of the Q&P treated martensitic stainless steel exhibit a larger arc diameter compared to the AISI 420. Bode plots show a higher impedance value for the Q&P treated steels compared to AISI 420 at the low frequency of 10^{-2} Hz. From the Bode plot, the minimum |Z| value at the low-frequency region means that the passive film for AISI 420 exhibits the lowest barrier properties for the passive films. A comparison between corrosion performance of Q&P treated martensitic stainless steels can be done. The QT113 steel has the smallest arc diameter and the lowest bode impedance at 10^{-2} Hz. It shows the lowest protective passive layer among all Q&P treated martensitic stainless steels. On the other hand, for the QT183 and QT205 steels, the arc diameters and the impedance values at the low frequency of 10^{-2} Hz is quite close to each other and higher than the QT155 and QT220 steels.

The Bode |Z| plots of all samples show linear slope in the intermediate frequencies that are associated with the double-layer capacitance. The phase angle plots show the non-ideal nature of the capacitance as the minimum phase angle is

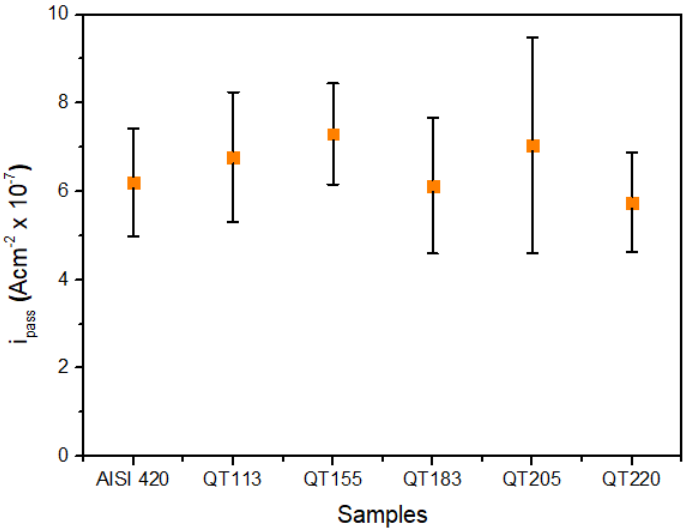

Figure 4.5: Passivation current density (i_{pass}) of the stainless steel samples based on potentiodynamic polarization curves.

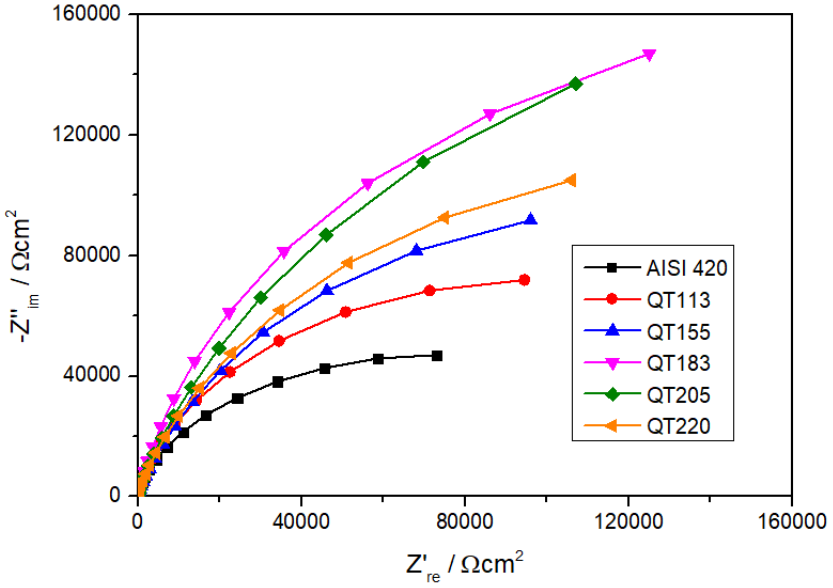

Figure 4.6: Nyquist plots of commercial martensitic stainless steel (AISI 420) and Q&P treated martensitic stainless steels in 3.5 wt.% NaCl solution.

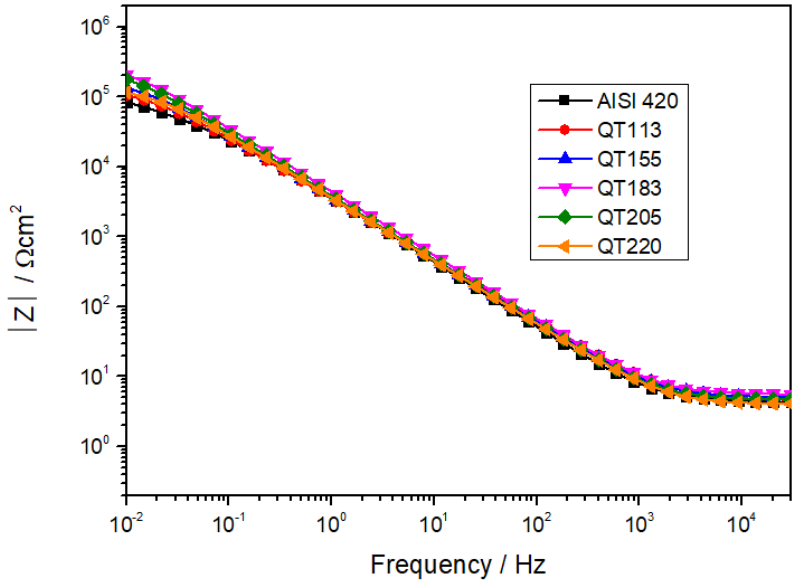

Figure 4.7: Bode impedance plots of commercial martensitic stainless steel (AISI 420) and Q&P treated martensitic stainless steels in 3.5 wt.% NaCl solution.

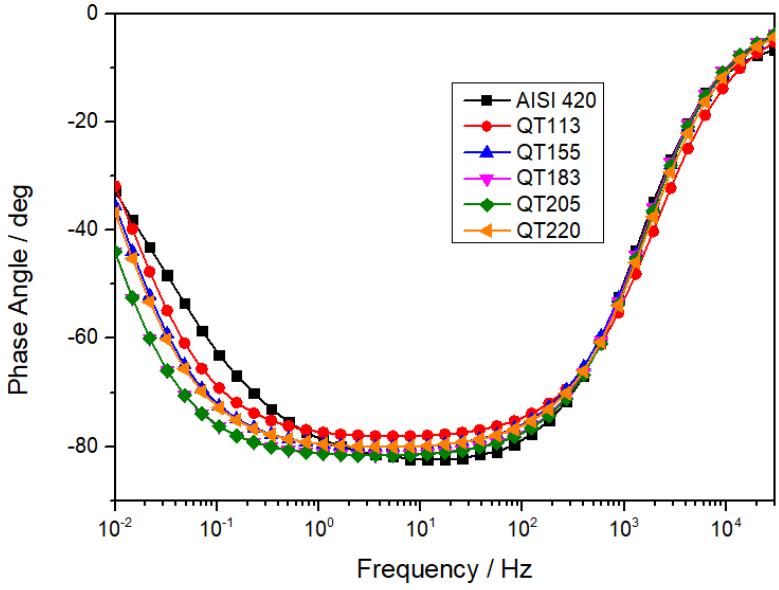

Figure 4.8: Phase angle plot of commercial martensitic stainless steel (AISI 420) and Q&P treated martensitic stainless steels in 3.5 wt.% NaCl solution.

slightly far from pure capacitor behaviour (-90°). This non-ideal behaviour can be explained by the imperfect nature (heterogeneities or roughness) of the electrode surface [54]. The experimental data fitted using an equivalent electrical circuit is illustrated in Figure 4.9, to elaborate the EIS results. This equivalent circuit has been used in previous works to describe the passive layer of similar systems [55, 56].

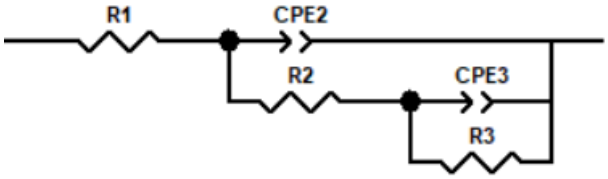

Figure 4.9: Equivalent circuit proposed for modelling the electrochemical response of commercial martensitic stainless steel (AISI 420) and Q&P treated martensitic stainless steels.

An equivalent circuit with two Constant Phase Elements (CPE) in parallel provides the best fitting for impedance data. CPEs are used instead of a perfect capacitance due to the deviation from the ideal capacitive behaviour. In the equivalent circuit, R_1 represents the resistance of the electrolyte. R_2 and CPE_2 are associated with the resistive and capacitive behaviour of the double layer (at higher frequencies), respectively. R_3 and CPE_3 are associated with the resistive and capacitive behaviour of the passive layer (at lower frequencies), respectively. The equivalent circuit fitting results are given in Table 4.3.

Table 4.3: The fitting values of the equivalent circuit components for AISI 420 and Q&P processed martensitic stainless steels.

Sample ID	R_1 (Ωcm^2)	CPE_2-Q ($\Omega^{-1}s^n cm^2 x10^{-5}$)	CPE_2-n	R_2 ($k\Omega cm^2$)	CPE_3-Q ($\Omega^{-1}s^n cm^2 x10^{-5}$)	CPE_3-n	R_3 ($k\Omega cm^2$)	X^2 (10^{-3})
AISI 420	3.46 ± 0.32	5.57 ± 0.51	0.92 ± 0.01	35.74 ± 11.72	4.54 ± 0.58	0.58 ± 0.02	89.64 ± 54.29	1.32 ± 0.62
QT113	4.76 ± 0.82	4.73 ± 0.55	0.92 ± 0.06	20.08 ± 5.09	1.94 ± 0.58	0.58 ± 0.02	155.38 ± 42.15	3.14 ± 2.21
QT155	4.89 ± 0.34	4.82 ± 0.57	0.92 ± 0.02	21.52 ± 3.98	1.97 ± 0.22	0.57 ± 0.08	205.38 ± 22.25	2.67 ± 1.23
QT183	5.32 ± 0.28	4.48 ± 0.54	0.91 ± 0.02	52.58 ± 10.52	1.92 ± 0.26	0.52 ± 0.03	324.23 ± 67.75	2.26 ± 1.81
QT205	4.54 ± 0.24	4.02 ± 0.12	0.93 ± 0.05	42.22 ± 4.82	1.72 ± 0.42	0.59 ± 0.09	313.57 ± 42.45	2.68 ± 1.64
QT220	4.69 ± 0.62	4.15 ± 0.24	0.93 ± 0.03	20.51 ± 3.26	1.67 ± 0.24	0.58 ± 0.04	267.04 ± 28.52	2.74 ± 1.57

The resistive behaviour of the passive film (R_3) for the Q&P treated steel microstructure is better than the annealed AISI 420. Among all Q&P treated steels, QT183 steel exhibits the highest R_3 value. From QT113 to QT183 with increasing quenching temperature, the R_3 value is increasing proportionally with the increasing retained austenite fraction. Then a drop in R_3 value is observed with increasing quenching temperature from QT205 to QT220. In addition, the differences can be seen clearly from Table 4.3 between the charge transfer resistance values of the double layer (R_2) and the passive layer (R_3). R_2 is lower than R_3, indicating that the resistive behaviour of the double layer is lower than the passive layer. Calculated CPE values are similar for both Q&P and AISI 420 microstructures. CPE_2-n values of all microstructures show similar capacitive behaviour of around 0.92. It means that the electrochemical behaviour of the double layer formed on the stainless steel samples slightly deviates from a pure capacitive (CPE_2-n = 1) behaviour.

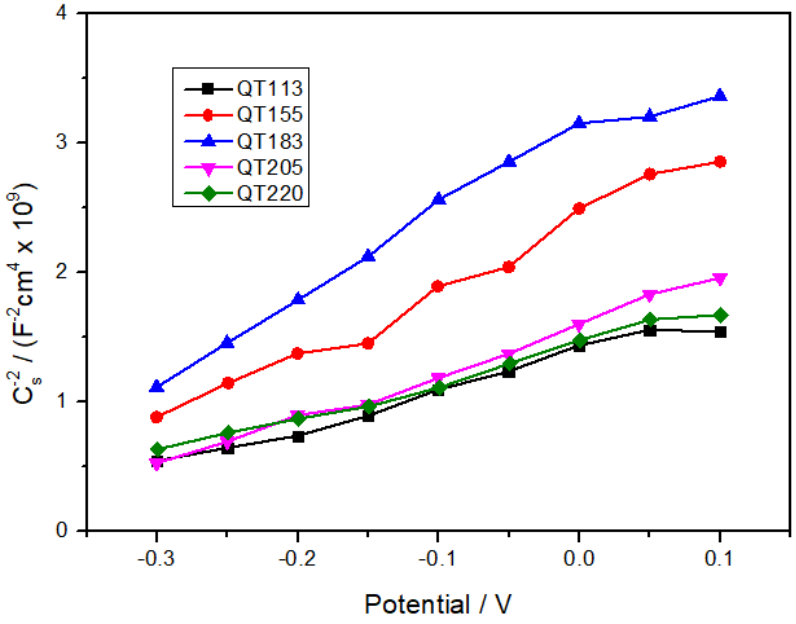

Figure 4.10: Mott-Schottky plots for the passive film formed on Q&P treated martensitic stainless steels in 3.5 wt.% NaCl solution.

In conclusion, Q&P treated martensitic stainless steels exhibit better corrosion performance in a chloride rich environment than the AISI 420, retained austenite and carbon-depleted primary martensite play a positive role together to reduce the corrosion rate of the Q&P treated steels. In addition, the resistive behaviour of the passive film has more contribution to corrosion behaviour compared to the resistive behaviour of the double layer.

Capacitance Measurements

The semiconducting properties of the passive films are investigated by Mott-Schottky analysis. Figure 4.10 shows the Mott-Schottky plots of the Q&P treated martensitic stainless steel. In Mott-Schottky plots, the positive slope indicates an n-type semiconductor behaviour of the passive films [57]. The slope of the Mott-Schottky plot is inversely related to the defectiveness of the passive films. As a result, the highest slope in the Mott-Schottky plot means the lowest defect density, better passive film properties.

A semiconductor-electrolyte interface consists of charged layers both on the semiconductor and electrolyte side, as shown in Figure 4.11 [58]. Passive film capacitance is influenced by the space charge region of the semiconductor and the Helmholtz double layer of the electrolyte. The film capacitance is the combination of the space charge region (SCR) and the Helmholtz double-layer (HL). The capac-

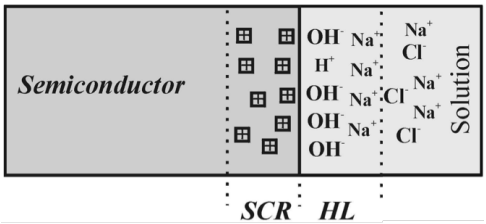

Figure 4.11: Space charge region (SCR) and Helmholtz (HL) double layer at the semiconductor-electrolyte interface [58].

itance of the SCR is much smaller than HL and the total capacitance of the passive film can be regarded as the capacitance of the SCR [59]. The donor density of the passive layer formed on Q&P steels can be calculated through Eq. 4.1.

$$C^{-2} = \frac{2(E - E_{FB} - \frac{kT}{e})}{\varepsilon\varepsilon_0 e N_d} \tag{4.1}$$

In Eq. 4.1, N_d is the donor density, C the capacitance, E_{FB} the flat band potential, k the Boltzmann constant, T the temperature, e the charge of electron, ε_0 the permittivity in vacuum, $\varepsilon = 15.6$ [36, 60] is the dielectric constant of the passive films formed on stainless steel.

The donor densities and flat band potential of the Q&P treated martensitic stainless steels are shown in Table 4.4. The flat band potential of the samples was calculated from the x-axis intercept of the Mott-Schottky plots.

Table 4.4: Donor density and flat band potential values obtained from Mott-Schottky analysis.

Sample ID	Donor density / N_d ($10^{21} cm^{-3}$)	Flat band potential (vs Ag/AgCl) / V
QT113	2.64 $\pm$ 0.3	-0.433 $\pm$ 0.05
QT155	1.65 $\pm$ 0.2	-0.421 $\pm$ 0.02
QT183	1.52 $\pm$ 0.2	-0.414 $\pm$ 0.01
QT205	2.38 $\pm$ 0.5	-0.426 $\pm$ 0.04
QT220	2.62 $\pm$ 0.2	-0.432 $\pm$ 0.01

The higher the number of donor density, the more defects within the passive film. The presence of defects makes the passive film susceptible to rupture (by deteriorating the passive layer properties), causing the pitting corrosion to initiate. From the capacitance results, QT113 steel is particularly more defective compared to the rest of the Q&P treated steels and the lowest donor density value belongs to QT183 steel. QT113 steel donor density value is 1.74 times the value of the QT183 steel. The lowest donor density value for the QT183 steel can be explained by the high amount of retained austenite and primary martensite phases. Among all Q&P treated steels, QT113, QT155 and QT183 have relatively low fresh martensite content compared to the QT205 and QT220 samples and these fresh martensite rich

steels (QT205 and QT220) exhibit worse passive film properties compared to the QT155 and QT183. The differences in the flat band potentials represent different passive film compositions as reported previously for the iron oxide volume fractions of the passive films on dual-phase carbon steel [61]. However, no significant difference was observed in the flat band potentials of Q&P treated martensitic stainless steels.

Depending on the dominant defects either p-type (Cr-rich inner layer) and/or n-type (Fe-rich outer layer) semiconductor behaviour can be observed in the passive film of stainless steels. In stainless steel, cation vacancy dominant passive films generally behave as p-type. On the other hand, cation interstitials or anion vacancy (oxygen ion) dominant films behave as n-type semiconductors. From the capacitance measurements, no evidence for p-type behaviour was obtained, indicating that as characteristics of the oxide (n-type), cation interstitials and/or oxygen ion vacancies are dominant defects. However, it is not possible to distinguish the contribution of oxygen vacancies and cation interstitials [36].

4.3. Passive Layer Analysis

X-ray photoelectron spectroscopy (XPS) measurements were performed to analyze the chemical composition of different oxide layers in the passive layer film (formed on contact with air) of Q&P treated martensitic stainless steels. For the XPS analysis, QT113 and QT183 were selected to see the effect of passive film composition on the passivation properties. High-resolution Fe 2p photoelectron spectra of QT113 and QT183 samples are given in Figure 4.12 and 4.13. High-resolution Cr 2p spectra for QT113 and QT183 is given in Figure 4.14 and 4.15. From Figure 4.12 and 4.13, it is possible to make comments about the Fe contribution. According to the literature, the peak position values of Fe 2p3/2 is between 710.6 and 711.2 eV. The binding energies of Fe 2p3/2 and Fe 2p1/2 obtained from the present study are 710.6 $\pm$ 0.009 and 724.1 $\pm$ 0.11 eV, respectively and these peaks represent Fe (III) oxide. The satellite peak (occur due to a sudden change in Coulombic potential as the photo-ejected electron passes through the valence band) was obtained at 718.8 $\pm$ 0.014 eV and it does not overlap with Fe 2p3/2 and Fe 2p1/2. The satellite peak of Fe 2p3/2 for Fe (III) oxide is located approximately 8 eV higher than the Fe 2p3/2 peak. [62, 63].

From Figure 4.14 and 4.15, it is possible to explain the Cr contribution. From literature, according to the XPS results corresponding to Cr 2p1/2 and Cr 2p3/2 orbitals, the peak appeared at binding energies of between 576.0 and 578.0 eV for Cr 2p3/2 and the peak appeared at binding energies of between 586.0 and 588.0 eV for Cr 2p1/2 orbital, these peaks represent Cr (III) oxide. The binding energies of Cr 2p3/2 and Cr 2p1/2 obtained from the present study are 576.4 $\pm$ 0.03 and 586.2 $\pm$ 0.08 eV, respectively. In addition, a satellite peak was observed for QT113 steel and no satellite peak was observed for QT183. According to the literature, the satellite peak of Cr 2p1/2 for Cr (III) oxide is located at 597 eV and in this study, the satellite peak is located at 596.6 eV [63, 64].

The phase fractions for Fe 2p are given in Table 4.5. The Fe (III) oxide contribution is similar for both Q&P treated QT113 and QT183 steels. The phase fractions for Cr 2p are calculated according to fitting parameters and given in Table 4.6. From the phase fraction results, the Cr/Fe oxide ratio from the most characteristics oxide (the ratio between Cr (III) oxide 2p3/2 and Fe (III) oxide 2p3/2) is for the QT113 steel (Cr/Fe oxide = 0.84) is lower than the QT183 steel (Cr/Fe oxide = 1.12). Due to this reason, the QT183 steel exhibits better passive film properties compared to the QT113 steel since the higher fraction of Cr oxide compared to Fe oxide is better for passivity properties. In addition to Fe 2p and Cr 2p, phase fractions for O 1s are calculated but no significant difference is observed (both samples have the same fraction oxide/hydroxides). As a conclusion, concerning the semiconductive behaviour of the passive films of Q&P treated martensitic stainless steel, it is possible to make comments about the duplex structure (Fe and Cr oxides) of the films. The duplex structure of the passive film is a combination of a chromium-rich (Cr (III)) oxide and an iron-rich (Fe (III)) oxide but the contribution of the chromium-rich layer is more critical for better corrosion performance.

Table 4.5: Fractions of the passive layer calculated from the fitting of Fe 2p spectrum.

	Fe metal (%) Fe 2p3/2	Fe (III) oxide (%) Fe 2p3/2	Satellite (%) Fe 2p3/2	Fe (III) oxide (%) Fe 2p1/2
QT113	3.29	65.36	3.52	27.83
QT183	4.00	62.04	3.67	30.29

Table 4.6: Fractions of the passive layer calculated from the fitting of Cr 2p spectrum.

	Cr (III) oxide (%) Cr 2p3/2	Cr (III) oxide (%) Cr 2p 1/2	Satellite (%) Cr 2p1/2
QT113	55.29	35.62	9.09
QT183	69.38	30.62	-

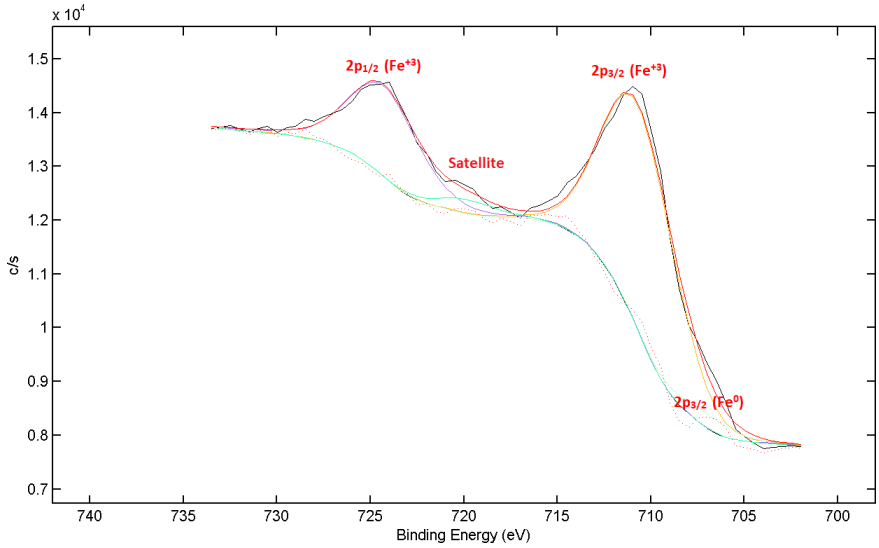

Figure 4.12: Experimental Fe 2p spectrum from the XPS measurement and corresponding fitting of the spectrum for the QT113.

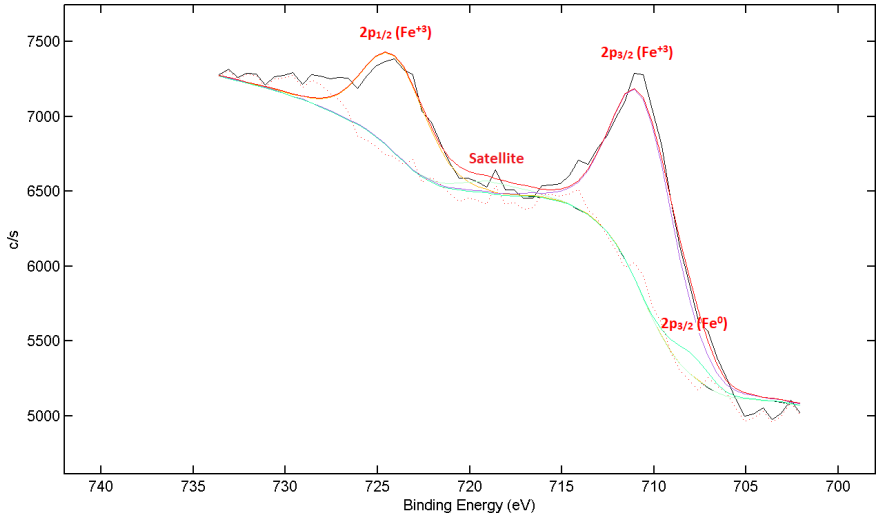

Figure 4.13: Experimental Fe 2p spectrum from the XPS measurement and corresponding fitting of the spectrum for the QT183.

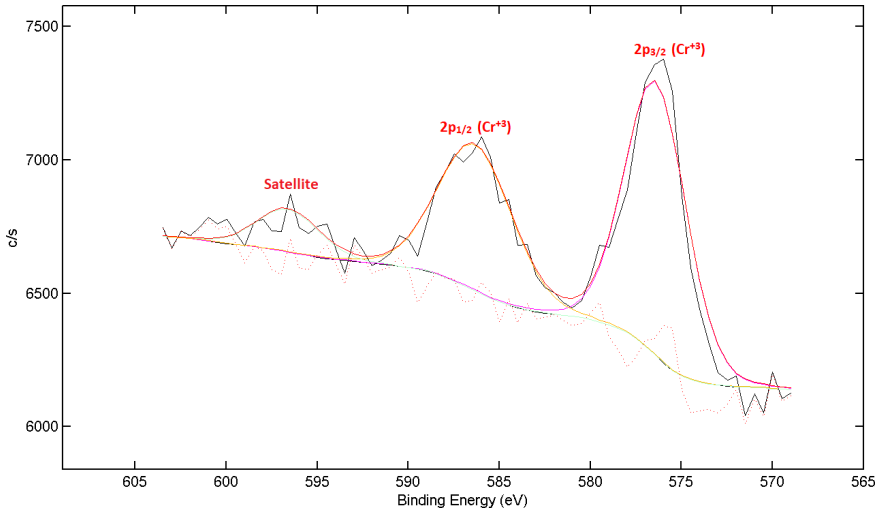

Figure 4.14: Experimental Cr 2p spectrum from the XPS measurement and corresponding fitting of the spectrum for the QT113.

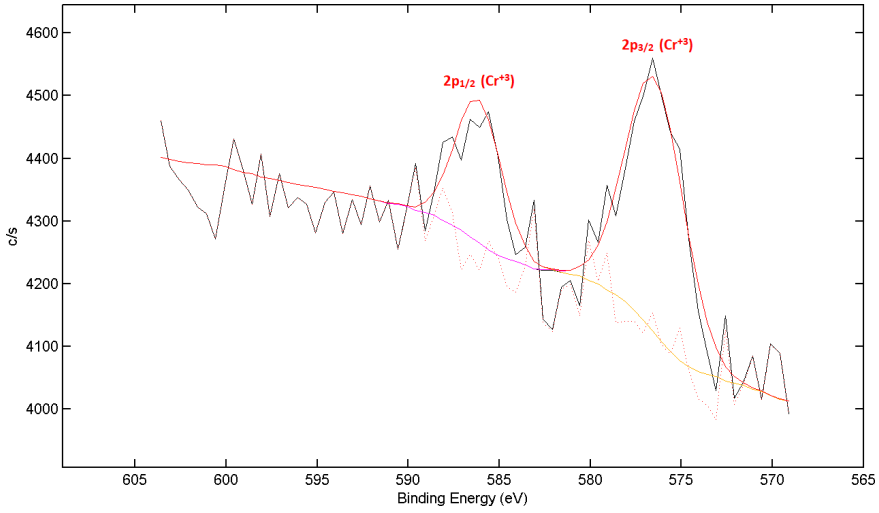

Figure 4.15: Experimental Cr 2p spectrum from the XPS measurement and corresponding fitting of the spectrum for the QT183.

4.4. Phase Dependency of Corrosion and Passivity

This section discusses the results of the electrochemical experiments. In particular, the corrosion response of the Q&P treated martensitic stainless steels and the passivity behaviour of these steels is discussed and compared with an annealed commercial martensitic stainless steel (AISI 420).

Results reveal that the AISI 420 steel corrodes slightly faster than the Q&P treated steel. The corrosion current density (i_{corr}) value for the AISI 420 is slightly higher than the Q&P treated martensitic stainless steels. A comparison between corrosion performance of Q&P treated martensitic stainless steels can be done. The lowest corrosion current density belongs to QT183 steel among all Q&P treated martensitic stainless steels. The current density value for QT113, QT155 and QT183 steels is lower than QT205 and QT220 steels. For the QT113, QT155 and QT138 steels, the fresh martensite content is insignificant compared to the QT205 and QT220 samples. This behaviour suggests that the presence of retained austenite and primary martensite (with partitioning decreases its carbon content and reduces its lattice distortion) phases contribute to better corrosion performance compared to the fresh martensite. Unlike primary martensite, fresh martensite is formed via final quench to room temperature from austenite with carbon content higher than the nominal content of the steel. Consequently, primary martensite contains fewer defects compared to fresh martensite [65]. Due to this reason, the higher corrosion current density for the QT205 and QT220 steels can be correlated with the high amount of defective fresh martensite. The defective structure of the fresh martensite can deteriorate the corrosion properties of Q&P treated martensitic stainless steels.

Except for the QT113 steel, all Q&P treated martensitic stainless steels have higher pitting potential (E_{pit}) compared to the AISI 420. This behaviour can be explained by the presence of carbides in the microstructure of the annealed AISI 420. The presence of carbides as heterogeneity is the preferential site for the pit initiation in the passive film and the initiation of the pit is followed by the breakdown of the passive layer which deteriorates the corrosion resistance.

It has been investigated that the corrosion resistance of the austenite phase is higher than ferrite/martensite [21, 51], due to that austenite contains lower internal stress and fewer defects [52]. Therefore, the distribution of the retained austenite might affect the pitting resistance of the Q&P treated martensitic stainless steels. The residual stress of the martensitic grain would be released when the less stressed retained austenite is well distributed in the microstructure [53], with this way the Q&P treated steels with less residual stresses (well distributed) would be more resistant to localized corrosion.

The resistance value of the passive layer (R_3) is higher for the Q&P treated steels compared to the AISI 420. The passive layer that formed on the Q&P treated steel microstructure is more corrosion resistant than the annealed AISI 420 steel. This behaviour suggests that the presence of carbides in the annealed AISI 420 deteriorate the corrosion properties. On the other hand, in Q&P treated steels, the presence of retained austenite and primary martensite contributes to the formation of better passive film layer properties. The carbon-depleted primary martensite and retained austenite play a positive role together to reduce the corrosion rate of the Q&P treated martensitic stainless steels, the serious carbon depletion of primary martensite via partitioning decreases lattice distortions and lower the residual stresses. In addition, retained austenite can easily tolerate the shape change caused by the martensitic transformation, further relaxation of internal stresses in retained austenite decreases the corrosion rate [66]. Thus, the relaxation of internal stresses in both primary martensite and retained austenite decreases the corrosion rate. In addition, the carbon-depleted primary martensite and retained austenite have less defective structure, thus the passive film properties are more protective.

Capacitance measurements can be used to make comments about the semiconducting behaviour of passive films that formed on Q&P treated martensitic stainless steels. From the Mott-Schottky results of Q&P treated martensitic stainless steels, no evidence for p-type behaviour (Cr-rich oxides) was obtained, indicating that as a characteristic of the passive film (n-type (Fe-rich oxides)), cation interstitials and/or oxygen ion vacancies are dominant defects [36]. Among all Q&P treated steels, the lowest donor density value belongs to the QT183 steel. Retained austenite fraction for QT183 steel is relatively high compared to the rest of the Q&P steels and the combination of less defective phases (primary martensite/retained austenite) makes the passive film more protective. On the other hand, the QT205 and QT220 steels exhibit worse passive film properties compared to the QT155 and QT183, due to the highly defective (high defect density) fresh martensite content in their microstructure.

XPS measurements were performed to analyze the chemical composition of different oxide layers in the passive film of Q&P treated martensitic stainless steels. From the XPS results, it is possible to observe Cr (III) and Fe (III) oxide peaks. The Cr/Fe oxide ratio is for the QT113 steel (Cr/Fe oxide = 0.84) is lower than the QT183 steel (Cr/Fe oxide = 1.12) and the higher fraction of Cr oxide is better for passivity properties. Due to this reason, QT113 steel with the highest donor density exhibits worse passive film performance compared to the QT183 steel with the lowest donor density. As a result, XPS results of the QT113 and Q183 are fitting well with the capacitance measurements.

In conclusion, the presence of retained austenite and primary martensite phases in Q&P treated martensitic stainless steels contribute better corrosion performance compared to the annealed commercial martensitic stainless steel (AISI 420). Among all Q&P treated steels, for the QT113, QT155 and QT183 steels, the fresh martensite content is insignificant compared to the QT205 and QT220 samples. From QT113 to QT183 with increasing quenching temperature, the E_{pit} from polarization curves and the R_3 value from impedance curves are increasing proportionally with the increasing retained austenite fraction and the i_{corr} value from polarization curves and the donor density values from capacitance measurements are decreasing with the increasing retained austenite fraction. For the fresh martensite rich samples (QT205 and QT220), the i_{corr} values and the donor density values are higher compared to the QT155 and QT183 steels, this trend can be explained with the presence of defective fresh martensite. In addition, it is not possible to ignore the effect of carbides or inclusions on the corrosion behaviour of Q&P treated steels. There might be carbides in the fresh martensite rich regions and/or the presence of inclusions deteriorate the corrosion performance of Q&P treated martensitic stainless steels.

5

Conclusions and Recommendations

5.1. Conclusions

For the automotive industry, the development in Q&P treated martensitic stainless steels can be a game-changer. The mechanical properties of Q&P treated commercial martensitic stainless steels have been widely investigated to combine strength with formability. The Q&P process of martensitic stainless steel can improve the mechanical properties by combining the strength of the martensite with the ductility of the retained austenite. Unlike mechanical behaviour, the corrosion response of Q&P treated martensitic stainless steel has not been investigated deeply. This thesis investigated the effect of microstructure on the corrosion and passivation behaviour of Q&P treated martensitic stainless steels.

For electrochemical measurements, six different samples were used. Out of these 6 samples, 5 of them (Q&P steels) had different volume fractions of retained austenite and martensite (tempered, fresh). One of them is an annealed commercial martensitic stainless steel (AISI 420). As an experimental path, open circuit potential, potentiodynamic polarization, electrochemical impedance spectroscopy (EIS) were performed in 3.5 wt.% NaCl to understand the corrosion properties of all samples. Mott-Schottky analysis and X-ray photoelectron spectroscopy (XPS) was performed to reveal the passive film properties of Q&P treated steels.

- For all samples, open-circuit potential shifts to more positive values, which is indicative of the passive film formation.
- Electrochemical impedance spectroscopy experiments show that all samples have similar capacitive behaviour. Nyquist plots of the Q&P treated martensitic stainless steels exhibit a larger arc diameter compared to the AISI 420 steel. Among all Q&P treated, QT113 steel has the smallest arc diameter and the lowest bode impedance at the lowest frequency. On the other hand, for the

QT183 and QT205 steels, the arc diameters and the impedance values are quite close to each other and higher than the QT155 and QT220 steels.

- The resistance value of the passive layer (R_3) for the Q&P treated steel microstructure is higher compared to the AISI 420. The passive layer that formed on the Q&P treated steels microstructure is more resistant than the AISI 420 steel. This behaviour suggests that the retained austenite and primary martensite phases contribute to the formation of a better passive film.
- Results reveal that the corrosion current density (i_{corr}) value for the AISI 420 is slightly higher than the Q&P treated martensitic stainless steels. Among all Q&P treated martensitic stainless steels, the lowest corrosion current density belongs to QT183 steel. The carbon-rich retained austenite and carbon-depleted primary martensite play a positive role together to reduce the corrosion rate of the Q&P treated steels. The serious depletion of carbon from primary martensite during partitioning reduces the residual stresses. In addition, the retained austenite can tolerates easily the shape change caused by the martensitic transformation, the relaxation of internal stresses in both primary martensite and retained austenite decreases the corrosion rate.
- The pitting potential (E_{pit}) is improved with the Q&P treatment. Except for the QT113, all Q&P treated martensitic stainless steels have higher E_{pit} compared to the AISI 420.
- From the capacitance measurements, no evidence for p-type behaviour was obtained, indicating that cation interstitials and/or oxygen ion vacancies are dominant defects in the passive film (n-type).
- The lowest donor density value for the QT183 steel can be explained by the high amount of retained austenite and primary martensite phases. The combination of less defective phases (primary martensite and retained austenite) makes the passive film more protective compared to the fresh martensite rich samples.
- From the XPS results, the Cr/Fe oxide ratio is for the QT113 steel is lower than the QT183 steel. Due to this reason, QT183 steel with the lowest donor density exhibits better corrosion performance compared to the QT113 steel.

The presented results indicate that the electrochemical behaviour of Q&P treated martensitic stainless steel is dependent on the phase constituents of the microstructure.

5.2. Recommendations

Recommendations for future research can be summarised as:

- The effect of microstructure on the corrosion performance of Q&P treated martensitic stainless steel microstructures can be studied in different environments other than NaCl to gain extensive knowledge.
- The effect of prior austenite grains size (PAGS) on the corrosion and passivation properties of Q&P treated martensitic stainless steel can be studied by changing the austenitization parameters.
- The analysis of the microstructural features with localized electrochemical methods such as Scanning Kelvin Probe Force Microscopy (SKPFM) could explain the Volta potential differences between phases to investigate the microgalvanic coupling.
- The presence of carbides in Q&P treated martensitic stainless steel microstructures can be studied with Transmission Electron Microscopy (TEM) to obtain detailed information about the pitting corrosion mechanism.

References

[1] D. K. Matlock and J. G. Speer, *Third Generation of AHSS: Microstructure Design Concepts,* Microstructure and Texture in Steels , 185 (2009).

[2] J. Speer, D. K. Matlock, B. C. De Cooman, and J. G. Schroth, *Carbon partitioning into austenite after martensite transformation,* Acta Materialia **51**, 2611 (2003).

[3] J. Mola and B. C. De Cooman, *Quenching and partitioning (Q&P) processing of martensitic stainless steels,* Metallurgical and Materials Transactions A: Physical Metallurgy and Materials Science **44**, 946 (2013).

[4] T. Tsuchiyama, J. Tobata, T. Tao, N. Nakada, and S. Takaki, *Microstructure control of a low carbon martensitic stainless steel by quenching and partitioning heat treatment,* Materials Science Forum **706-709**, 2338 (2012).

[5] J. Tobata, K. L. Ngo-Huynh, N. Nakada, T. Tsuchiyama, and S. Takaki, *Role of silicon in quenching and partitioning treatment of lowcarbon martensitic stainless steel,* ISIJ International **52**, 1377 (2012).

[6] H. Bhadeshia and R. Honeycombe, *STEELS Microstructure and Properties* (2017).

[7] C. Lerchbacher, S. Zinner, and H. Leitner, *Direct or indirect: Influence of type of retained austenite decomposition during tempering on the toughness of a hot-work tool steel,* Materials Science and Engineering A **564**, 163 (2013).

[8] E. Koufis, *A study of the effect of prior austenite grain size on the microstructure of Quenching and Partitioning steels with Phase-Field Modelling,* (2020).

[9] J. G. Speer, E. De Moor, K. O. Findley, D. K. Matlock, B. C. De Cooman, and D. V. Edmonds, *Analysis of microstructure evolution in quenching and partitioning automotive sheet steel,* Metallurgical and Materials Transactions A: Physical Metallurgy and Materials Science **42**, 3591 (2011).

[10] T. Tsuchiyama, J. Tobata, T. Tao, N. Nakada, and S. Takaki, *Quenching and partitioning treatment of a low-carbon martensitic stainless steel,* Materials Science and Engineering A **532**, 585 (2012).

[11] M. Hillert and J. Ågren, *On the definitions of paraequilibrium and orthoequilibrium,* Scripta Materialia **50**, 697 (2004).

[12] M. Hillert and J. Ågren, *Reply to comments on "On the definition of paraequilibrium and orthoequilibrium",* Scripta Materialia **52**, 87 (2005).

[13] Q. Huang, C. Schröder, H. Biermann, O. Volkova, and J. Mola, *Influence of Martensite Fraction on Tensile Properties of Quenched and Partitioned (Q&P) Martensitic Stainless Steels,* Steel Research International **87**, 1082 (2016).

[14] M. Tisza, *Development of Lightweight Steels for Automotive Applications,* Engineering Steels and High Entropy-Alloys , 1 (2020).

[15] G. Luo, H. Li, Y. Li, and J. Mo, *Low-Carbon-Chromium Ferritic Stainless Steel,* (2019), 10.3390/ma12101704.

[16] Q. Huang, O. Volkova, B. C. De Cooman, H. Biermann, and J. Mola, *Influence of Si addition on the carbon partitioning process in martensitic-austenitic stainless steels,* IOP Conference Series: Materials Science and Engineering **373** (2018), 10.1088/1757-899X/373/1/012001.

[17] J. Ning, Y. Zheng, B. Brown, D. Young, and S. Nešić, *A thermodynamic model for the prediction of mild steel corrosion products in an aqueous hydrogen sulfide environment,* Corrosion **71**, 945 (2015).

[18] B. N. Popov, *Corrosion Engineering: Principles and Solved Problems* (2015).

[19] S. A. Refaey, F. Taha, and A. M. Abd El-Malak, *Corrosion and inhibition of 316L stainless steel in neutral medium by 2-mercaptobenzimidazole,* International Journal of Electrochemical Science **1**, 80 (2006).

[20] R. T. Loto, *Pitting Corrosion Resistance and Inhibition of Lean Austenitic Stainless Steel Alloys,* Austenitic Stainless Steels - New Aspects (2017), 10.5772/intechopen.70579.

[21] I. Taji, M. H. Moayed, and M. Mirjalili, *Correlation between sensitisation and pitting corrosion of AISI 403 martensitic stainless steel,* Corrosion Science **92**, 301 (2015).

[22] R. Fan, M. Gao, Y. Ma, X. Zha, X. Hao, and K. Liu, *Effects of Heat Treatment and Nitrogen on Microstructure and Mechanical Properties of 1Cr12NiMo Martensitic Stainless Steel,* Journal of Materials Science and Technology **28**, 1059 (2012).

[23] J. Burja, B. Šuler, M. Češnjaj, and A. Nagode, *Effect of intercritical annealing on the microstructure and mechanical properties of 0.1c-13cr-3ni martensitic stainless steel,* Metals **11**, 1 (2021).

[24] Y. Zhou and D. L. Engelberg, *Accessing the full spectrum of corrosion behaviour of tempered type 420 stainless steel,* Materials and Corrosion (2021), 10.1002/maco.202112442.

[25] E. Mabruri, R. R. Pasaribu, M. T. Sugandi, and Sunardi, *Effect of high temperature tempering on the mechanical properties and microstructure of the modified 410 martensitic stainless steel,* AIP Conference Proceedings **1964** (2018), 10.1063/1.5038314.

[26] M. Mirzaee, A. Momeni, N. Aieni, and H. Keshmiri, *Effect of quenching and tempering on microstructure and mechanical properties of 410 and 410 Ni martensitic stainless steels,* Journal of Materials Research **32**, 687 (2017).

[27] K. Morshed-Behbahani, N. Zakerin, P. Najafisayar, and M. Pakshir, *A survey on the passivity of tempered AISI 420 martensitic stainless steel,* Corrosion Science **183**, 109340 (2021).

[28] Y. Zhao, W. Liu, Y. Fan, T. Zhang, B. Dong, L. Chen, and Y. Wang, *Influence of microstructure on the corrosion behavior of super 13Cr martensitic stainless steel under heat treatment,* Materials Characterization **175**, 111066 (2021).

[29] J. Yang, Y. Lu, Z. Guo, J. Gu, and C. Gu, *Corrosion behaviour of a quenched and partitioned medium carbon steel in 3.5 wt.% NaCl solution,* Corrosion Science **130**, 64 (2018).

[30] T. Mehner, R. Morgenstern, P. Frint, I. Scharf, M. F. Wagner, and T. Lampke, *Corrosion characteristics of a quenching and partitioning steel determined by electrochemical impedance spectroscopy,* IOP Conference Series: Materials Science and Engineering **373** (2018), 10.1088/1757-899X/373/1/012003.

[31] S. Dieck, M. Ecke, T. Halle, and P. Rosemann, *Improvement of the martensitic stainless steel X46Cr13 by Q&P heat treatment,* IOP Conference Series: Materials Science and Engineering **882** (2020), 10.1088/1757-899X/882/1/012006.

[32] S. Y. Lu, K. F. Yao, Y. B. Chen, M. H. Wang, N. Chen, and X. Y. Ge, *Effect of quenching and partitioning on the microstructure evolution and electrochemical properties of a martensitic stainless steel,* Corrosion Science **103**, 95 (2016).

[33] Y. b. Guo, C. Li, Y. c. Liu, L. m. Yu, Z. q. Ma, C. x. Liu, and H. j. Li, *Effect of microstructure variation on the corrosion behavior of high-strength low-alloy steel in 3.5wt% NaCl solution,* International Journal of Minerals, Metallurgy and Materials **22**, 604 (2015).

[34] S. Marcelin, N. Pébère, and S. Régnier, *Electrochemical characterisation of a martensitic stainless steel in a neutral chloride solution,* Electrochimica Acta **87**, 32 (2013).

[35] M. J. Carmezim, A. M. Simões, M. F. Montemor, and M. Da Cunha Belo, *Capacitance behaviour of passive films on ferritic and austenitic stainless steel,* Corrosion Science **47**, 581 (2005).

[36] A. Fattah-Alhosseini, A. Saatchi, M. A. Golozar, and K. Raeissi, *The passivity of AISI 316L stainless steel in 0.05 M H2SO 4,* Journal of Applied Electrochemistry **40**, 457 (2010).

[37] K. D. Ralston and N. Birbilis, *Effect of grain size on corrosion: A review,* Corrosion **66**, 0750051 (2010).

[38] W. R. Osório, L. C. Peixoto, L. R. Garcia, and A. Garcia, *Electrochemical corrosion response of a low carbon heat treated steel in a NaCl solution,* Materials and Corrosion **60**, 804 (2009).

[39] A. Fattah-Alhosseini and S. Vafaeian, *Influence of grain refinement on the electrochemical behavior of AISI 430 ferritic stainless steel in an alkaline solution,* Applied Surface Science **360**, 921 (2016).

[40] M. Pisarek, P. Kędzierzawski, M. Janik-Czachor, and K. J. Kurzydłowski, *Effect of hydrostatic extrusion on passivity breakdown on 303 austenitic stainless steel in chloride solution,* Journal of Solid State Electrochemistry **13**, 283 (2009).

[41] A. A. Tiamiyu, U. Eduok, J. A. Szpunar, and A. G. Odeshi, *Corrosion behavior of metastable AISI 321 austenitic stainless steel: Investigating the effect of grain size and prior plastic deformation on its degradation pattern in saline media,* Scientific Reports **9**, 1 (2019).

[42] A. Fattah-Alhosseini and S. Vafaeian, *Comparison of electrochemical behavior between coarse-grained and fine-grained AISI 430 ferritic stainless steel by Mott-Schottky analysis and EIS measurements,* Journal of Alloys and Compounds **639**, 301 (2015).

[43] B. D. Bakker, *Influence of Quenching Temperature and Mn Content on the Microstructure Development of New Q & P Processed Martensitic Stainless Steels,* Repository TU Delft (2021).

[44] K. Andrews, *The calculation of transformation temperatures and austenite-ferrite equilibria in steels,* JISI **184**, 414 (1956).

[45] C. Y. Kung and J. J. Rayment, *An examination of the validity of existing empirical formulae for the calculation of ms temperature,* Metallurgical Transactions A **13**, 328 (1982).

[46] Q. Huang, H. Biermann, and J. Mola, *Influence of martensite fraction on the extent of partitioning in martensitic stainless steels processed by quenching and partitioning (Q&P),* 8th European Stainless Steel and Duplex Stainless Steel Conference 2015 , 389 (2015).

[47] Q. Huang, O. Volkova, H. Biermann, and J. Mola, *Dilatometry Analysis of Dissolution of Cr-Rich Carbides in Martensitic Stainless Steels,* Metallurgical and Materials Transactions A: Physical Metallurgy and Materials Science **48**, 5771 (2017).

[48] D. P. Koistinen and R. E. Marburger, *A general equation prescribing the extent of the austenite-martensite transformation in pure iron-carbon alloys and plain carbon steels,* Acta Metallurgica **7**, 59 (1959).

[49] S. M. Van Bohemen and J. Sietsma, *Effect of composition on kinetics of athermal martensite formation in plain carbon steels,* Materials Science and Technology **25**, 1009 (2009).

[50] J. G. Speer, F. C. Rizzo Assunção, D. K. Matlock, and D. V. Edmonds, *The "quenching and partitioning" process: Background and recent progress,* Materials Research **8**, 417 (2005).

[51] J. S. Lee, K. Fushimi, T. Nakanishi, Y. Hasegawa, and Y. S. Park, *Corrosion behaviour of ferrite and austenite phases on super duplex stainless steel in a modified green-death solution,* Corrosion Science **89**, 111 (2014).

[52] H. Hill, S. Huth, S. Weber, and W. Theisen, *Corrosion properties of a plastic mould steel with special focus on the processing route,* Materials and Corrosion **62**, 436 (2011).

[53] N. Luzginova, L. Zhao, and J. Sietsma, *Evolution and thermal stability of retained austenite in SAE 52100 bainitic steel,* Materials Science and Engineering A **448**, 104 (2007).

[54] L. Jinlong and L. Hongyun, *The effects of cold rolling temperature on corrosion resistance of pure iron,* Applied Surface Science **317**, 125 (2014).

[55] Z. J. Jia, C. W. Du, C. T. Li, Z. Yi, and X. G. Li, *Study on pitting process of 316L stainless steel by means of staircase potential electrochemical impedance spectroscopy,* International Journal of Minerals, Metallurgy and Materials **18**, 48 (2011).

[56] M. Sánchez, J. Gregori, C. Alonso, J. J. García-Jareño, H. Takenouti, and F. Vicente, *Electrochemical impedance spectroscopy for studying passive layers on steel rebars immersed in alkaline solutions simulating concrete pores,* Electrochimica Acta **52**, 7634 (2007).

[57] Y. Takabatake, K. Fushimi, T. Nakanishi, and Y. Hasegawa, *Grain-Dependent Passivation of Iron in Sulfuric Acid Solution,* Journal of The Electrochemical Society **161**, C594 (2014).

[58] C. Ozkan, *The Role of Phase Combinations on the Corrosion and Passivity Behaviour of High Strength Steels,* (2020).

[59] J. Kang, Y. Yang, X. Jiang, and H. Shao, *Semiconducting properties of passive films formed on electroplated Ni and Ni-Co alloys,* Corrosion Science **50**, 3576 (2008).

[60] A. Fattah-alhosseini, M. A. Golozar, A. Saatchi, and K. Raeissi, *Effect of solution concentration on semiconducting properties of passive films formed on austenitic stainless steels,* Corrosion Science **52**, 205 (2010).

[61] K. Yanagisawa, T. Nakanishi, Y. Hasegawa, and K. Fushimi, *Passivity of Dual-Phase Carbon Steel with Ferrite and Martensite Phases in pH 8.4 Boric Acid-Borate Buffer Solution,* Journal of The Electrochemical Society **162**, C322 (2015).

[62] T. Yamashita and P. Hayes, *Analysis of XPS spectra of Fe 2+ and Fe 3+ ions in oxide materials,* Applied Surface Science **254**, 2441 (2008).

[63] M. C. Biesinger, B. P. Payne, A. P. Grosvenor, L. W. Lau, A. R. Gerson, and R. S. C. Smart, *Resolving surface chemical states in XPS analysis of first row transition metals, oxides and hydroxides: Cr, Mn, Fe, Co and Ni,* Applied Surface Science **257**, 2717 (2011).

[64] A. M. Salvi, J. E. Castle, J. F. Watts, and E. Desimoni, *Peak fitting of the chromium 2p XPS spectrum,* Applied Surface Science **90**, 333 (1995).

[65] M. J. Santofimia, R. H. Petrov, L. Zhao, and J. Sietsma, *Microstructural analysis of martensite constituents in quenching and partitioning steels,* Materials Characterization **92**, 91 (2014).

[66] J. Yang, F. Huang, Z. Guo, Y. Rong, and N. Chen, *Effect of retained austenite on the hydrogen embrittlement of a medium carbon quenching and partitioning steel with refined microstructure,* Materials Science and Engineering A **665**, 76 (2016).